Max-Planck-Institut
für Meteorologie

REPORT No. 47

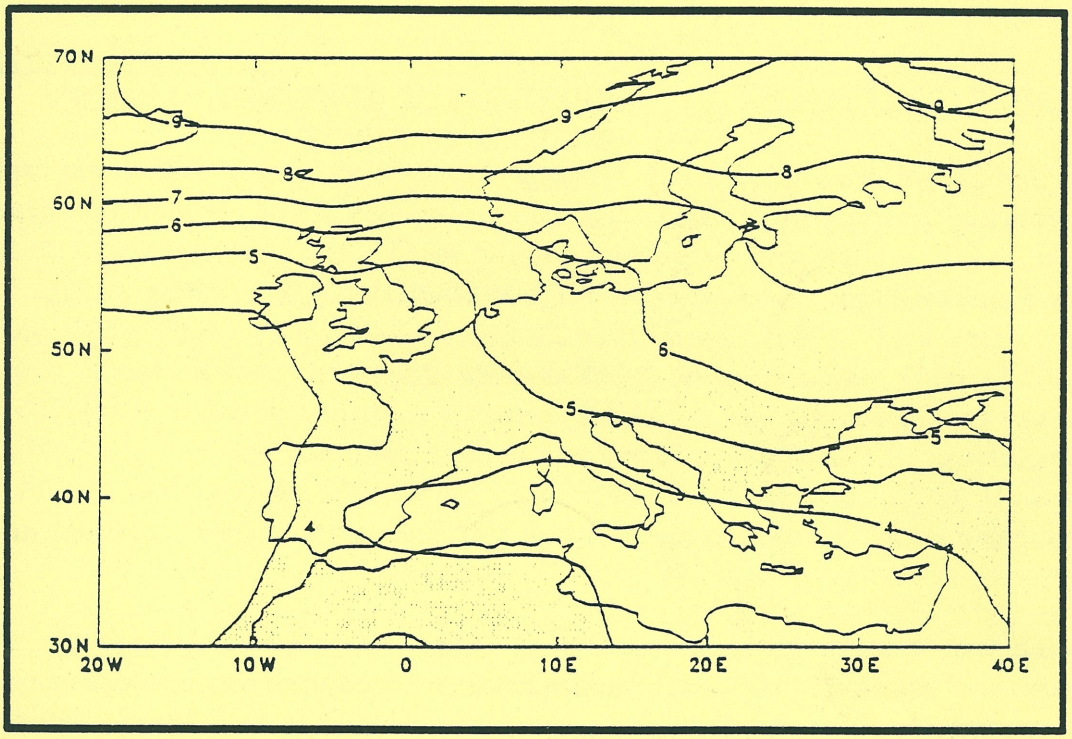

DEVELOPING CLIMATE SCENARIOS FROM EQUILIBRIUM GCM RESULTS

by

B.D. SANTER • T.M.L. WIGLEY
M.E. SCHLESINGER • J.F.B. MITCHELL

HAMBURG, MARCH 1990

AUTHORS:

BENJAMIN D. SANTER
MAX-PLANCK-INSTITUT
FUER METEOROLOGIE

TOM M.L. WIGLEY
CLIMATIC RESEARCH UNIT
UNIVERSITY OF EAST ANGLIA
NORWICH
NR4 7TJ
U.K.

MICHAEL E. SCHLESINGER
DEPARTMENT OF ATMOSPHERIC SCIENCES
UNIVERSITY OF ILLINOIS
URBANA
U.S.A.

JOHN F.B. MITCHELL
UNITED KINGDOM METEOROLOGICAL OFFICE
BRACKNELL
BERKS RG12 2SZ
U.K.

MAX-PLANCK-INSTITUT
FUER METEOROLOGIE
BUNDESSTRASSE 55
D-2000 HAMBURG 13
F.R. GERMANY

Tel.: (040) 4 11 73-0
Telex: 211092
Telemail: MPI.Meteorology
Telefax: (040) 4 11 73-298

REPb47

ISSN 0937–1060

Developing Climate Scenarios From Equilibrium GCM Results

B.D. Santer[1], T.M.L. Wigley[2], M.E. Schlesinger[3] and J.F.B. Mitchell [4]

[1] Max-Planck-Institut für Meteorologie, Bundesstrasse 55, 2 Hamburg 13, West Germany
[2] Climatic Research Unit, University of East Anglia, Norwich, NR4 7TJ, U.K.
[3] Department of Atmospheric Sciences, University of Illinois, Urbana, U.S.A.
[4] United Kingdom Meteorological Office, Bracknell, Berks RG12 2SZ, U.K.

1 Introduction

In the last ten years, a number of major international studies have attempted to assess the potential impacts of climate change induced by increasing atmospheric concentrations of CO_2 and other greenhouse gases. These studies considered impacts in a variety of sectors, e.g. agriculture, energy and water resources, forestry, fisheries, etc. (National Academy of Sciences, 1983; Parry et al., 1988a,b; Smith and Tirpak, 1989). To a greater or lesser extent, such climate impact investigations have relied on output from General Circulation Models (GCMs) in order to construct scenarios for future climate change. Other methods are available for generating scenarios, such as the use of paleoclimatic or instrumental data analogs (Pittock and Salinger, 1982; Lough et al., 1983; Palutikof et al., 1984). However, only GCMs can provide the space-time resolution and richness of information required by impact analysts.

This does not imply that a state-of-the-art GCM can supply the 'correct' four-dimensional picture of the atmospheric response to doubled atmospheric CO_2. There are four reasons why we should only regard current GCMs as instruments for making intelligent guesses (and not predictions) about the climate system's response to specified forcings:

- Although GCMs solve the same primitive equations, each model represents a different, highly individual solution to the problem of modelling the Earth's climate. Each GCM can be regarded as an individual species within the genus of climate models. There are large inter-model differences in resolution and physics, particularly in the treatment of clouds, sea ice and land surface processes and in the representation of the ocean. These differences explain why there is substantial disagreement in the regional details of the equilibrium response to doubled CO_2 (Schlesinger and Mitchell, 1987).
- All climate models still have systematic errors in their simulations of present-day climate (von Storch et al., 1985; Grotch, 1988; Santer and Wigley, 1990).

- There are large uncertainties in modelling the oceans and cloud properties, in the coupling of atmosphere and ocean models, and in other sub-grid scale parameterizations. The implication of these uncertainties is that current climate models are unlikely to incorporate all the physical processes and feedback mechanisms that are necessary to reliably simulate the climate impact of greenhouse-gas forcing.

- Most of our knowledge concerning the regional and seasonal details of the climate response to greenhouse-gas forcing has been obtained from equilibrium response experiments. These are experiments which consider the steady-state response of the model's climate to a step-function change in atmospheric CO_2. In the real world, we are more concerned with the time-dependent response to time-dependent greenhouse-gas forcing. Recent evidence from the few GCM experiments that have been performed with time-dependent greenhouse-gas forcing (so-called *transient* experiments) suggests that there may be important differences between the equilibrium and transient responses (Hansen et al., 1988; Bryan et al., 1988; Washington and Meehl, 1989, Stouffer et al., 1989).

Increasingly, impact analysts are requesting model data with higher spatial and temporal resolution. The demand is for scenarios with greater 'richness of information' – i.e., for variables with direct relevance for impact analysis (e.g. evapotranspiration, maximum and minimum temperature, runoff), and for information on changes in variances and the frequency of extreme events. Impact studies are now being performed at the regional level, often for individual states or countries (e.g., Pittock and Nix, 1986; Gleick, 1987; Parry et al., 1988a,b; Smith and Tirpak, 1989) and sometimes using daily data (Wilks, 1988). These studies generally rely on results from one or several GCMs. Given the lack of regional reliability and the fact that a scenario is not meant to be a prediction, this approach is reasonable. An alternative approach would be to make use of all available equilibrium response results (e.g., from CO_2 experiments with comparable levels of atmosphere-ocean interaction). This allows the impact analyst to assess uncertainty (in the sense of inter-model differences) and to easily produce a range of scenarios.

2 Method

The scenarios which we will produce are for two seasons (DJF, JJA) and two variables (surface air temperature and precipitation rate). Data are from equilibrium response experiments performed with the following GCMs:

- Goddard Institute for Space Studies (GISS; Hansen et al., 1984)
- National Center for Atmospheric Research (NCAR; Washington and Meehl, 1984)
- Geophysical Fluid Dynamics Laboratory (GFDL; Wetherald and Manabe, 1986)
- United Kingdom Meteorological Office (UKMO; Wilson and Mitchell; 1987)
- Oregon State University (OSU; Schlesinger and Zhao; 1989)

The models listed above comprise all available simulations that employ mixed-layer oceans and comparable levels of atmosphere-ocean interaction. Details of some relevant model properties are given in Table 1. The OSU GCM has the smallest horizontal resolution, 4° latitude x 5° longitude, and this is the grid we have used for the temperature and precipitation scenarios. Results from the other four models were transformed to this grid using a Gaussian filter. The domain is global; selected regional scenarios are given in Section 3.

2.1 Temperature Scenarios

The simplest temperature scenario which utilizes results from all five models is the 'model average' of the $2xCO_2$ minus $1xCO_2$ change in surface air temperature, $\Delta\overline{T}$. If ΔT_i is the $2xCO_2$ minus $1xCO_2$ temperature change for model i at a given grid-point,

$$\Delta\overline{T} = \frac{1}{n}\sum_{i=1}^{n}\Delta T_i \tag{1}$$

where $n = 5$ is the number of models. The geographical distribution of $\Delta\overline{T}$ (Figure 1) shows the classical equator-to-pole amplification of the temperature change in the winter hemisphere, a feature which is common to each of the five models used here.

However, the model average alone can be misleading, and results may be dominated by a single model. For example, we know that the NCAR GCM has maximum values of ΔT_i in JJA that are displaced ca. 5° equatorward relative to the warming maxima of the other models (Schlesinger and Mitchell, 1987). The NCAR results will dominate in this region. Since it is probable that the NCAR GCM's equatorward displacement of warming maxima is erroneous[1], the equatorward extension of warming maxima in the model average may be spurious.

The model average, therefore, can mask information about the degree of model-to-model variability. This information can be obtained by comparing the results from individual models or by using some measure of inter-model variability. A simple measure of the uncertainty of $\Delta\overline{T}$ is the unbiased estimate of the model-to-model standard deviation, $\hat{s}_1$, where

$$\hat{s}_1^2 = \sum_{i=1}^{n}\left(\Delta T_i - \Delta\overline{T}\right)^2/(n-1) \tag{2}$$

Ideally, we would like to have a large number of independent realizations of the ΔT_i fields for computing $\hat{s}_1$. Here we have only a limited sample of five models. Figure 2 shows that the inter-model variability is largest ($\hat{s}_1 > 6°C$) at high latitudes in the winter hemisphere, particularly at sea-ice margins.

A simple measure of the signal strength (i.e., the magnitude of $\Delta\overline{T}$) relative to the model-to-model noise level is given by the ratio SN1, where

$$SN1 = \Delta\overline{T}/\hat{s}_1 \tag{3}$$

[1] Due to an unrealistic control run sea-ice distribution, with the ice extent too far north.

The geographical distribution of SN1 provides spatial information on the level of agreement between models (Figure 3). The ratio is generally larger over oceans than over land areas, and is largest over the subtropical oceans. The smallest values of SN1, indicating poor inter-model agreement, are located at sea-ice margins and in continental interiors. SN1 has the advantage that the level of inter-model agreement can be compared directly for different variables (such as temperature and precipitation).

2.2 Standardized Temperature Scenarios

The model averages for the winter and summer patterns of temperature change in Figure 1 may be biased by the different equilibrium sensitivities (ΔT_{eq}) of the five models,[2] which range from 2.8°C (OSU) to 5.2°C (UKMO; see Table 1). To produce temperature scenarios which remove this bias, the seasonal temperature change at each grid-point in each model is expressed as a fraction of the model's equilibrium sensitivity, $\Delta T_{eq(i)}$. These fractions are then averaged. This 'standardized' model average, $\Delta\overline{T}^*$ is given by

$$\Delta\overline{T}^* = \frac{1}{n}\sum_{i=1}^{n}\left(\Delta T_i/\Delta T_{eq(i)}\right) \tag{4}$$

The geographical distribution of the standardized model average is given in Figure 4. Its level of uncertainty is expressed by the model-to-model standard deviation of the fractional changes, $\hat{s}_2$, where

$$\hat{s}_2^2 = \sum_{i=1}^{n}\frac{\left[\left(\Delta T_i/\Delta T_{eq(i)}\right) - \Delta\overline{T}^*\right]^2}{n-1} \tag{5}$$

The spatial distribution of $\hat{s}_2$ (Figure 5) shows that there is considerable agreement between models in terms of the patterns of $\Delta T_i/\Delta T_{eq(i)}$. For both seasons, the model-to-model standard deviation of the fractional changes is less than 25% of the model average equilibrium sensitivity, $\Delta\overline{T}_{eq}$ (3.94°C) over most of the globe.

As in (3), we can obtain a simple estimate of the signal strength (the magnitude of $\Delta\overline{T}^*$) relative to the model-to-model noise level by computing the ratio SN2, where

$$SN2 = \Delta\overline{T}^*/\hat{s}_2 \tag{6}$$

(see Figure 6).

There are two reasons why the scenarios given in Figure 4 are superior to the straight model average. First, the use of fractions of ΔT_{eq} produces results which capture the *patterns* of temperature change without being biased by different model equilibrium sensitivities. Second, we can now introduce a time dimension into the scenarios (see Section 3) through the time dependence of global mean annually-averaged temperature.

[2]The equilibrium or climate sensitivity is defined as the $2xCO_2$ minus $1xCO_2$ change in global mean annual average surface air temperature.

2.3 Precipitation Scenarios

The use of a model average precipitation scenario is not meaningful (Figure 7). For temperature, there is reasonable qualitative agreement in the model patterns of ΔT_i. This is not the case for precipitation. The patterns of $2xCO_2$ minus $1xCO_2$ changes in precipitation rate (ΔP_i) show large qualitative and quantitative differences, particularly between latitudes 30°S to 30°N. The model-to-model standard deviation of ΔP_i ($\hat{s}_1$) is as large as $\Delta\overline{P}$, the model average change in precipitation rate, over large areas of the tropics and subtropics (Figure 8). The ratio SN1 (not shown) is less than or equal to 1.0 over more than 50% of the global surface.

The poor regional agreement of ΔP_i patterns between 30°S to 30°N is partly attributable to model differences in the parameterization of cumulus convection and to differences in the conditions required for cloud formation (Schlesinger and Mitchell, 1987). It is also due to the fact that the natural variability of precipitation is large relative to the CO_2-induced change in precipitation. Significance tests performed with the $1xCO_2$ and $2xCO_2$ precipitation data from individual models (e.g., for the OSU model, see Schlesinger and Zhao, 1989, and Santer et al., 1990) indicate that significant responses in the precipitation field are confined to small areas – i.e., they are local rather than global.

We can have little confidence in a scenario based on the averaging of such disparate ΔP_i fields, particularly in the tropics and subtropics. The question, therefore, is whether we can use the available equilibrium ΔP_i results to generate precipitation scenarios that reflect model uncertainties in the simulation of precipitation. The method used here is to estimate the *probability* of a change in precipitation in a specific direction.

Consider a specific example (Table 2). At the grid-point 50°N, 100°W (located near Winnepeg) the values of $\Delta\overline{P}$ and $\hat{s}_1$ for JJA are 0.14 mm/day and 0.38 mm/day, respectively. All models except GFDL show an increase in precipitation. If we assume that the ΔP_i values for the individual models are random samples from a Gaussian distribution, the probability that $\Delta\overline{P}$ is less than zero can be calculated. For the values of $\Delta\overline{P}$ and $\hat{s}_1$ given in Table 2, the probability of a decrease in precipitation is given by $p = 0.36$ – i.e., the most likely result is an increase in precipitation. However, even though four of the five models agree qualitatively in this respect, the large inter-model differences mean that there is still a significant chance (about one in three) of a precipitation decrease.

The geographical distribution of the probability of a decrease in precipitation ($p_\Downarrow$) is given in Figure 9. This provides combined information about the direction of change (which at this stage of model development is all that we can hope to have confidence in) and the level of model-to-model variability. There are several obvious features. Despite the large decreases in ΔP_i in individual models in the tropics and subtropics (in both seasons), inter-model variability is large, so that there are only small areas where $p_\Downarrow$ is 0.9 or greater (e.g., the S.E. United States, Western Sahara and the sub-tropical N. Atlantic in winter). The values of $p_\Downarrow$ in winter are generally small (0.2 or less) poleward of 30°N and 30°S. In summer, $p_\Downarrow$ tends to be larger than in winter over land areas poleward of 30°N. This result primarily reflects the GFDL summertime precipitation decreases over large areas of Northern Hemisphere land

masses.

3 Timing of Future Changes

Equilibrium response results provide information about the steady-state response of a model's climate to a given level of forcing. The forcing in equilibrium response experiments is constant with time. As we have seen in the previous section, the $2xCO_2$ minus $1xCO_2$ change in global mean annually-averaged temperature (ΔT_{eq}) is the yardstick used for measuring the equilibrium sensitivity of different models. ΔT_{eq} depends critically on a variety of feedback processes which exist within the climate system. The feedback mechanisms likely to be important in determining ΔT_{eq} involve clouds, water vapor, sea ice, snow cover, ocean circulation, etc. Since the quantitative effects of these feedbacks are uncertain, the magnitude of ΔT_{eq} is also uncertain. The best estimate that we have for ΔT_{eq} is that it lies within the range 1.5 to 4.5°C (MacCracken and Luther, 1985; Bolin et al., 1986).

In the real world, however, we are concerned with the time-dependent response of the climate system to time-varying forcing by greenhouse gases. This is the transient response. The critical problem here is to account for the damping or lag effect of oceanic thermal inertia. Previous attempts to estimate the magnitude of such lag effects have used relatively simple one-dimensional models (see Hoffert and Flannery, 1985, for a review), or have used GCMs with mixed-layer oceans in which oceanic horizontal heat transport is prescribed and vertical transport out of the mixed-layer is approximated by diffusion (Hansen et al., 1988). To obtain better estimates of ocean lag effects we require transient experiments in which AGCMs are coupled with dynamic oceans with realistic horizontal and vertical transport of heat.

The lag between the equilibrium response and the transient response is determined by three factors:

- The climate sensitivity (model-dependent)
- Oceanic thermal inertia effects (model-dependent)
- The future rate of change of greenhouse gas concentrations

Present levels of uncertainty for the climate sensitivity, ocean lag effects and the greenhouse gas forcing have been summarized by Wigley (1989a,b). Based on these uncertainties, the global mean warming over the next 40 years is expected to be between 0.5°C and 2.5°C, with a best estimate of 1.5°C (Figure 10). We can use such estimates of the expected global mean warming to introduce a time dimension (including uncertainties) into the $\Delta\overline{T}^{*}$ scenarios presented in Section 2 (see Figure 4). Recall that in these scenarios, the different equilibrium sensitivities of the five individual models have been factored out.

The assumption on which this approach is based is that the spatial patterns of temperature change (which we have derived from GCM equilibrium response results) are stable in the

transition from $1xCO_2$ to $2xCO_2$. This is unlikely to be the case. Such scenarios represent a compromise pending the availability of model output from GCM transient experiments with dynamic oceans.

4 Regional Scenarios

The scenarios presented in Section 2 were global. Here, we provide scenarios for a North American study area (10°N-70°N; 50°W-140°W) and a European study area (30°N-70°N; 20°W-40°E). The results are derived as in Section 2 and are for:

- $\Delta\overline{T}$ Model average temperature change (Figures 11 and 15)
- $\Delta\overline{T}^*$ Standardized model average temperature change (Figures 12 and 16)
- SN2 Ratio of $\Delta\overline{T}^*/\hat{s}_2$; Figures 13 and 17)
- $p_\downarrow$ (probability of a decrease in precipitation; Figures 14 and 18)

Such scenarios can be easily produced for other regions and for the monthly time scale.

Acknowledgements

We wish to acknowledge the assistance of the modelling groups at GFDL, GISS and NCAR for providing equilibrium response data. Maps were produced with contouring routines written by J.M. Oberhuber at MPI.

References

Bolin, B., Döös, B.R., Jäger, J. and Warrick, R.A. (Eds.), 1986: *The Greenhouse Effect, Climatic Change, and Ecosystems.* SCOPE Vol. 29, John Wiley and Sons Ltd., Chichester, 539pp.

Bryan, K., Manabe, S. and Spelman, M.J., 1988: Interhemispheric asymmetry in the transient response of a coupled ocean-atmosphere model to a CO_2 forcing. *Journal of Physical Oceanography 18*, 851-867.

Gleick, P.H., 1987: Regional hydrologic consequences of increases in atmospheric CO_2 and other trace gases. *Climatic Change 10*, 137-161.

Grotch, S.L., 1988: Regional intercomparisons of general circulation model predictions and historical climate data. *U.S. Dept. of Energy, Carbon Dioxide Research Division, Report No. TR041.* Lawrence Livermore National Laboratory, Livermore, California, 291pp.

Hansen, J., Fung, I., Lacis, A., Rind, D., Lebedeff, S., Ruedy, R. and Russell, G., 1988: Global climate changes as forecast by Goddard Institute for Space Studies three-dimensional model. *Journal of Geophysical Research 93*, 9341-9364.

Hansen, J., Lacis, A., Rind, D., Russell, G., Stone, P., Fung, I., Ruedy, R. and Lerner, J., 1984: Climate sensitivity: Analysis of feedback mechanisms. In: *Climate Processes and Climate Sensitivity* (Eds. J. Hansen and T. Takahashi), pp 130-163. Maurice Ewing Series 5, American Geophysical Union, Washington D.C., 368 pp.

Hoffert, M.I. and Flannery, B.P., 1985: Model projections of the time-dependent response to increasing carbon dioxide. In: *Projecting the Climatic Effects of Increasing Carbon Dioxide.* U.S. Department of Energy, Carbon Dioxide Research Division, Washington D.C., 149-190.

Jones, P.D., Wigley, T.M.L. and Farmer, G., 1989: Changes in hemispheric and regional temperatures 1851 to 1988 over land and marine areas. In: *Proceedings of DOE Workshop on Greenhouse-Gas-Induced Climatic Change* (Ed. M.E. Schlesinger). In press.

Lough, J.M., Wigley, T.M.L. and Palutikof, J.P., 1983: Climate and climate impact scenarios for a warmer world. *Journal of Climate and Applied Meteorology 22*, 1673-1684.

MacCracken, M.C. and Luther, F.M., 1985: *Projecting the Climatic Effects of Increasing Carbon Dioxide.* U.S. Department of Energy, Carbon Dioxide Research Division, Washington D.C., 381pp.

Meehl, G.A. and Washington, W.M., 1989: CO_2 climate sensitivity and snow-sea-ice albedo parameterizations in an atmospheric GCM coupled to a mixed-layer ocean model. Submitted to *Climatic Change.*

Mitchell, J.F.B., Senior, C.A. and Ingram, W.J., 1989: CO_2 and climate: a missing feedback? *Nature 341*, 132-134.

National Research Council (NRC), 1983: *Changing Climate.* Report of the Carbon Dioxide Assessment Committee, National Academy Press, Washington D.C.

Palutikof, J.P., Wigley, T.M.L. and Lough, J.M., 1984: *Seasonal Scenarios for Europe and North America in a High-CO_2, Warmer World.* Technical Report TR012, U.S. Department of Energy, Carbon Dioxide Research Division, Washington D.C., 70pp.

Parry, M.L., Carter, T.R. and Konijn, N.T. (Eds.), 1988a: *The Impact of Climatic Variations on Agriculture. Volume 1: Assessments in Cool Temperate and Cold Regions.* Kluwer Academic Publishers, Dordrecht, 888pp.

Parry, M.L., Carter, T.R. and Konijn, N.T. (Eds.), 1988b: *The Impact of Climatic Variations on Agriculture. Volume 2: Assessments in Semi-Arid Regions.* Kluwer Academic Publishers,

Dordrecht, 800pp.

Pittock, A.B. and Nix, H.A., 1986: The effect of changing climate on Australian biomass production – a preliminary study. *Climatic Change 8*, 243-255.

Pittock, A.B. and Salinger, M.J., 1982: Towards regional scenarios for a CO_2-warmed Earth. *Climatic Change 4*, 23-40.

Santer, B.D., Wigley, T.M.L., Schlesinger, M.E. and Jones, P.D., 1990: Multivariate methods for the detection of greenhouse-gas-induced climate change. In: *Proceedings of DOE Workshop on Greenhouse-Gas-Induced Climatic Change* (Ed. M.E. Schlesinger). In press.

Santer, B.D. and Wigley, T.M.L., 1990: Regional validation of means, variances and spatial patterns in GCM control runs. *Journal of Geophysical Research*, in press.

Schlesinger, M.E. and Zhao, Z.-C., 1989: Seasonal climate changes induced by doubled CO_2 as simulated by the OSU atmospheric GCM mixed-layer ocean model. *Journal of Climate 2*, in press.

Schlesinger, M.E. and Mitchell, J.F.B., 1987: Climate model simulations of the equilibrium climatic response to increased carbon dioxide. *Reviews of Geophysics 25*, 760-798.

Smith, J.B. and Tirpak, D.A., 1989: *The Potential Effects of Global Climate Change on the United States*. Draft Report to Congress, U.S. EPA, June 1989.

von Storch, H., Roeckner, E. and Cubasch, U., 1985: Intercomparison of extended-range January simulations with general circulation models: Statistical assessment of ensemble properties. *Beiträge zur Physik der Atmosphäre 58*, 477-497.

Washington, W.M. and Meehl, G.A., 1989: Climate sensitivity due to increased CO_2: experiments with a coupled atmosphere and ocean general circulation model. *Climate Dynamics* 4, 1-38.

Washington, W.M. and Meehl, G.A., 1984: Seasonal cycle experiment on the climate sensitivity due to a doubling of CO_2 with an atmospheric general circulation model coupled to a simple mixed-layer ocean model. *Journal of Geophysical Research 89*, 9475-9503.

Wetherald, R.T. and Manabe, S., 1986: An investigation of cloud cover change in response to thermal forcing. *Climatic Change 8*, 5-23.

Wilks, D.S., 1988: Estimating the consequences of CO_2-induced climatic change on North American grain agriculture using general circulation model information. *Climatic Change 13*, 19-42.

Wilson, C.A. and Mitchell, J.F.B., 1987: A doubled CO_2 climate sensitivity experiment with a global climate model including a simple ocean. *Journal of Geophysical Research 92*, 13,315-13,343.

Wigley, T.M.L., 1989a: When will equilibrium CO_2 results be relevant? *Climate Monitor 17*,

99-106.

Wigley, T.M.L., 1989b: *The Greenhouse Effect: Scientific Assessment of Climate Change.* Lecture presented at the Prime Minister's seminar on Global Climate Change, 26 April 1989, U.K. Dept. of Environment, 18pp.

Table 1

Major Features of the Five GCMs

	GFDL	GISS	NCAR	OSU	UKMO
Horizontal resolution (lat. x long.)	4.44° x 7.5°	7.83° x 10.0°	4.44° x 7.5°	4.0° x 5.0°	5.0° x 7.5°
Vertical resolution (no. of layers)	9	9	9	2	11
Geography	realistic	realistic	realistic	realistic	realistic
Clouds	computed	computed	computed	computed	computed
Diurnal cycle	no	yes	no	no	yes
Base 1xCO_2 (ppm)	300	315	330	326	323
Solar constant (W/m^2)	1443.7	1367	1370	1354	1373
Maximum mixed layer depth (m)	68	65	50	60	50
ΔT_{eq} (°C)	4.0	4.2	3.5[a]	2.8	5.2[b]
ΔP (%)	8.7	11.0	7.1	7.8	15.0

[a] For the NCAR result, the control climate did not attain equilibrium (Washington and Meehl, 1984). An integration performed with a revised snow/sea-ice/albedo formulation attained equilibrium. The ΔT_{eq} from the latter experiment was 4.04°C (Meehl and Washington, 1989).

[b] For the UKMO case, recent experiments performed with different cloud prediction schemes have given ΔT_{eq} values of 1.9°C and 2.9°C (Mitchell et al., 1989).

Table 2

Precipitation Changes (JJA) at Grid-Point 50°N, 100°W

Model	ΔP_i (mm/day)
GFDL	-0.52
GISS	+0.45
NCAR	+0.18
OSU	+0.38
UKMO	+0.19
$\Delta\overline{P}$	+0.14
$\hat{s}_1$	0.38

Figure 1: Model average of the $2xCO_2$ minus $1xCO_2$ change in surface air temperature ($\Delta\overline{T}$). Results are for DJF (a) and JJA (b), and are computed using equilibrium response data from five GCMs (GFDL, GISS, NCAR, OSU and UKMO). The contour interval is 1°C. Shading denotes areas where $\Delta\overline{T}$ is greater than or equal to 5°C.

a

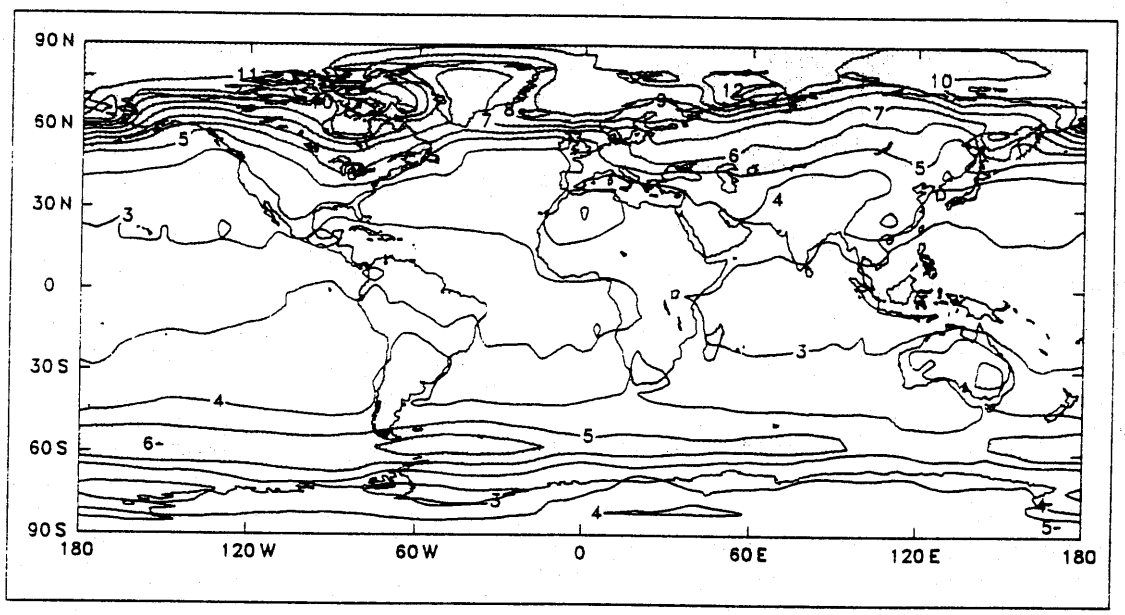

b

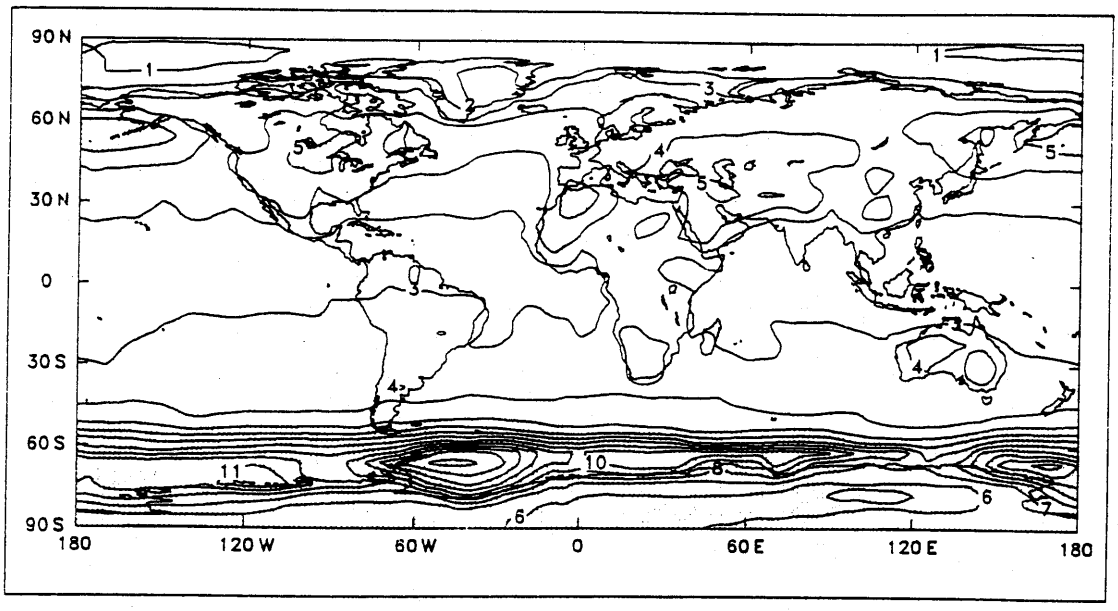

Figure 2: Model-to-model standard deviation ($\hat{s}_1$) of the $2xCO_2$ minus $1xCO_2$ change in surface air temperature. $\hat{s}_2$ is a measure of the uncertainty of $\Delta\overline{T}$. Results are for DJF (a) and JJA (b), and are computed using equilibrium response data from five GCMs. The contour interval is 1°C. Shading denotes areas where $\hat{s}_1$ is greater than or equal to 3°C.

a

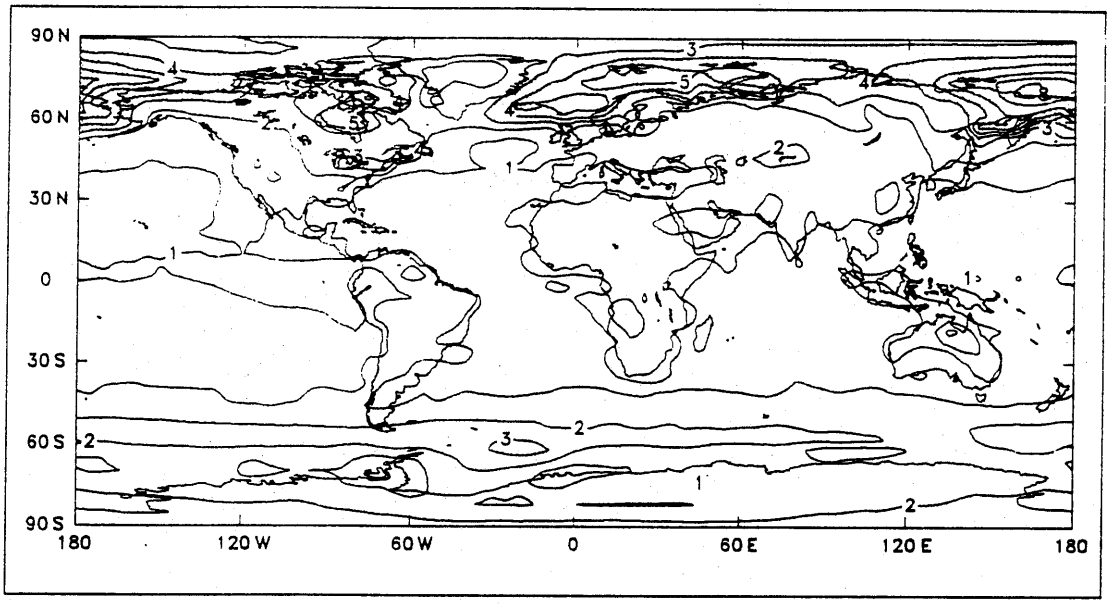

b

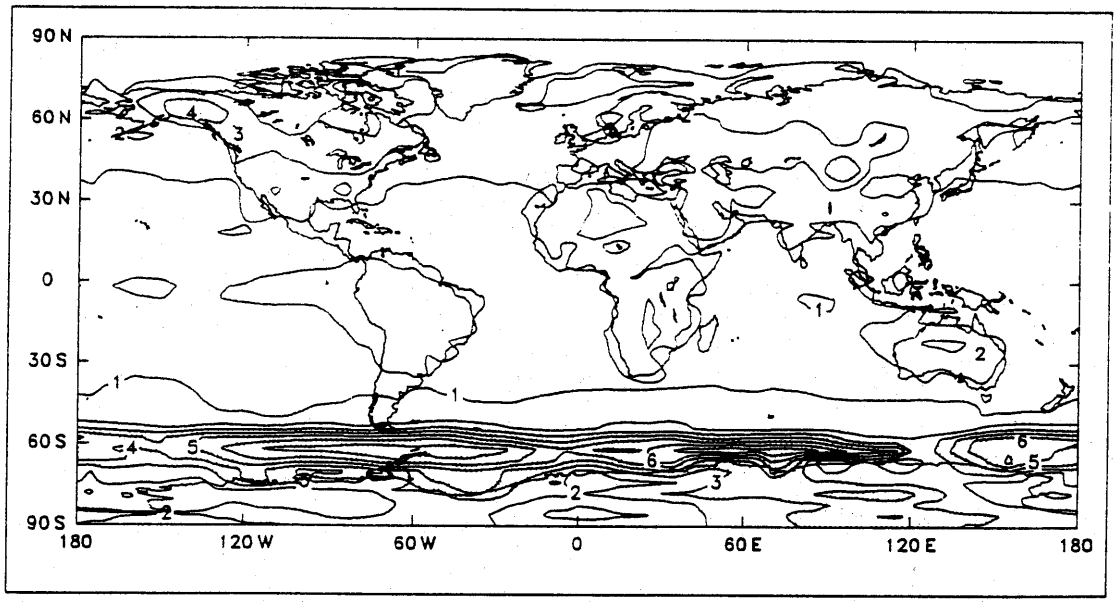

Figure 3: Signal-to-noise ratio SN1. SN1 is a measure of the magnitude of the model average temperature change ($\Delta\overline{T}$) relative to the model-to-model noise level ($\hat{s}_1$). Results are for DJF (a) and JJA (b), and are computed using equilibrium response data from five GCMs. The contour interval is 1. Shading denotes areas where SN1 is greater than or equal to 3. Note that SN1 is generally larger over oceans than over land areas, and is largest over the subtropical oceans.

a

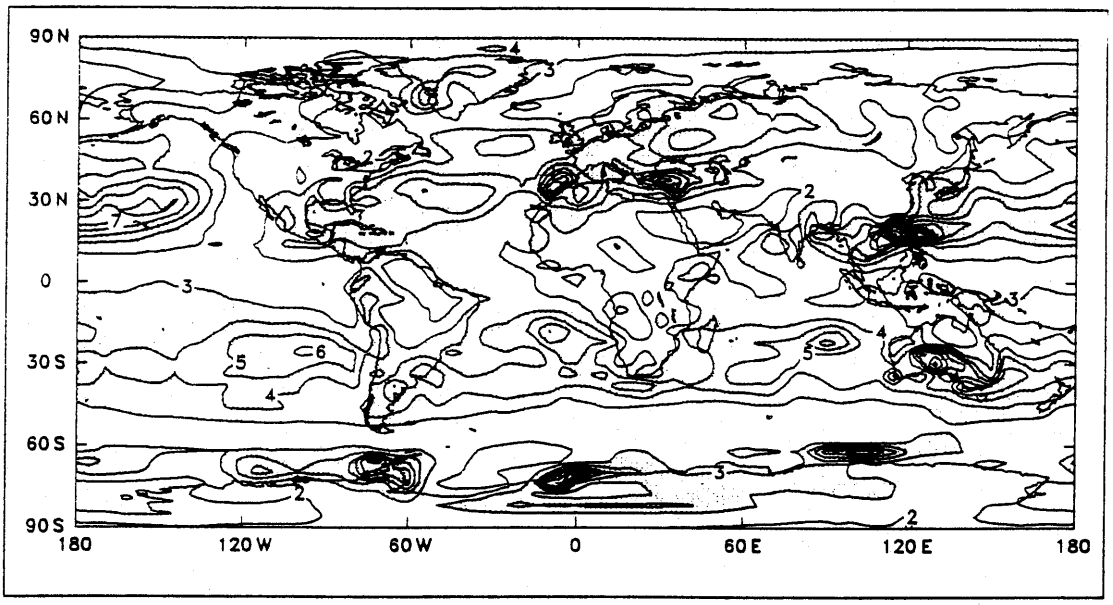

b

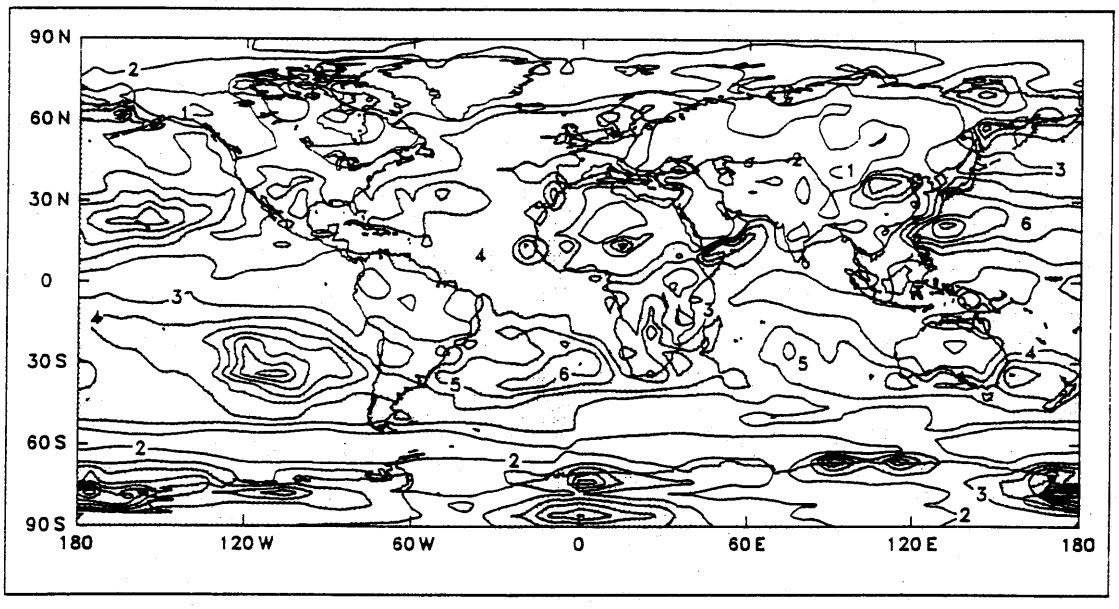

Figure 4: Standardized model average of the $2xCO_2$ minus $1xCO_2$ change in surface air temperature ($\Delta\overline{T}^*$). The seasonal temperature change at each grid-point in each model is expressed as a fraction of the model's equilibrium sensitivity, $\Delta T_{eq(i)}$. $\Delta\overline{T}^*$ is the average of the fractional changes (see Section 2.2). Results are for DJF (a) and JJA (b), and are computed using equilibrium response data from five GCMs. The contour interval is 0.5. Shading denotes areas where $\Delta\overline{T}^*$ is greater than or equal to 1.5. $\Delta\overline{T}^*$ captures the patterns of temperature change without being biased by different model equilibrium sensitivities.

a

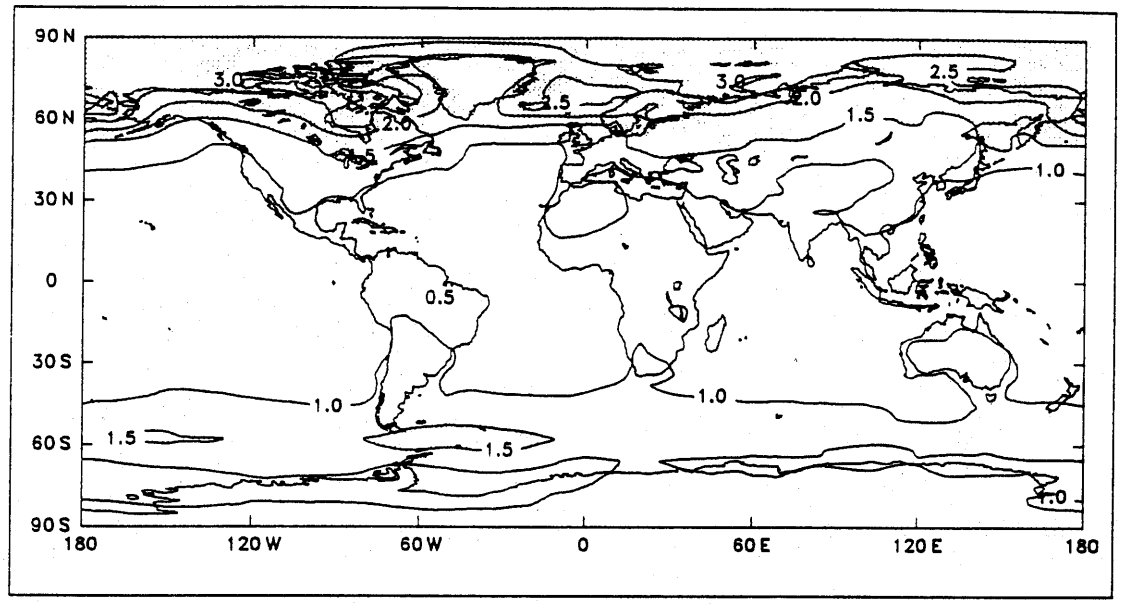

b

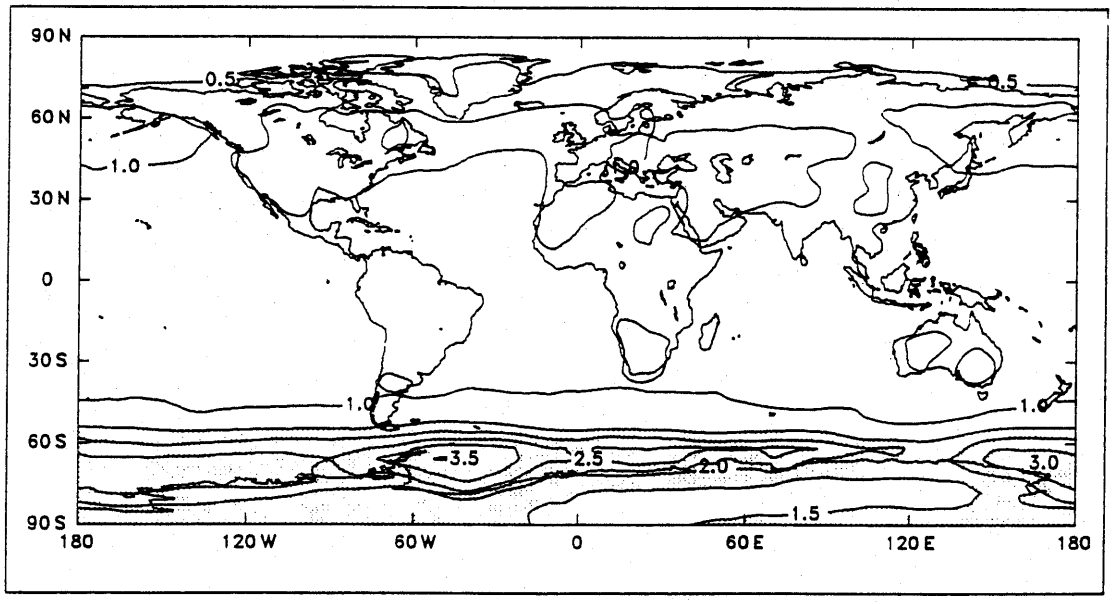

Figure 5: Model-to-model standard deviation ($\hat{s}_2$) of the fractional changes in surface air temperature ($\Delta T_i / \Delta T_{eq(i)}$). $\hat{s}_2$ is a measure of the uncertainty of $\Delta \overline{T}^*$. Results are for DJF (a) and JJA (b), and are computed using equilibrium response data from five GCMs. The contour interval is 0.25. Shading denotes areas where $\hat{s}_2$ is greater than or equal to 0.5.

a

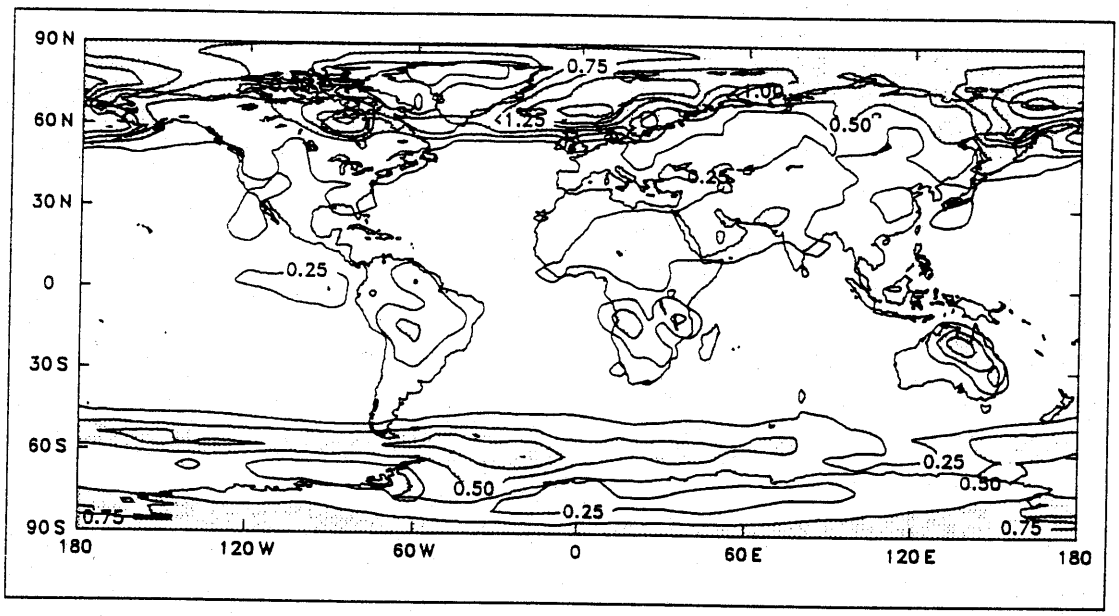

b

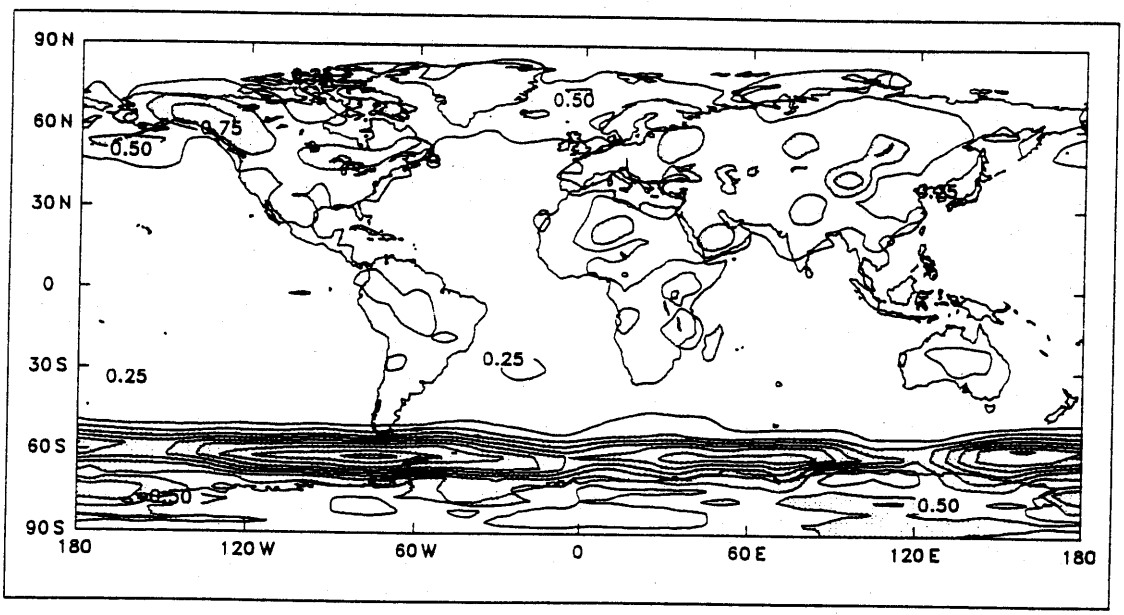

Figure 6: Signal-to-noise ratio SN2. SN2 is a measure of the magnitude of the standardized model average temperature change ($\Delta\overline{T}^*$) relative to the model-to-model noise level ($\hat{s}_2$). Results are for DJF (a) and JJA (b), and are computed using equilibrium response data from five GCMs. The contour interval is 5. Shading denotes areas where SN2 is greater than or equal to 5. SN2 is generally larger over oceans than over land areas, and is largest over subtropical oceans.

a

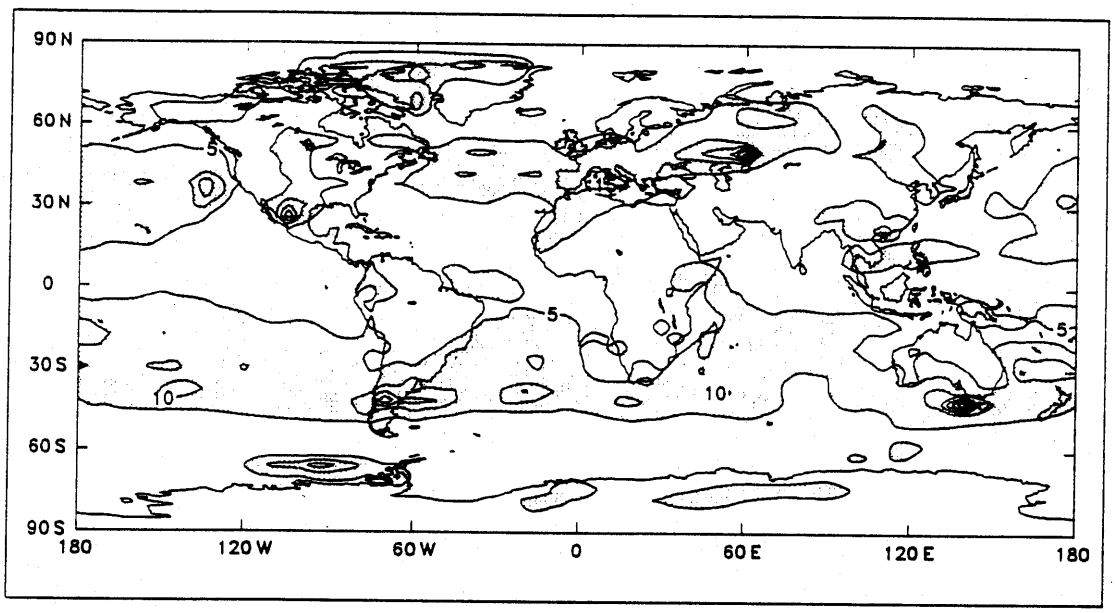

b

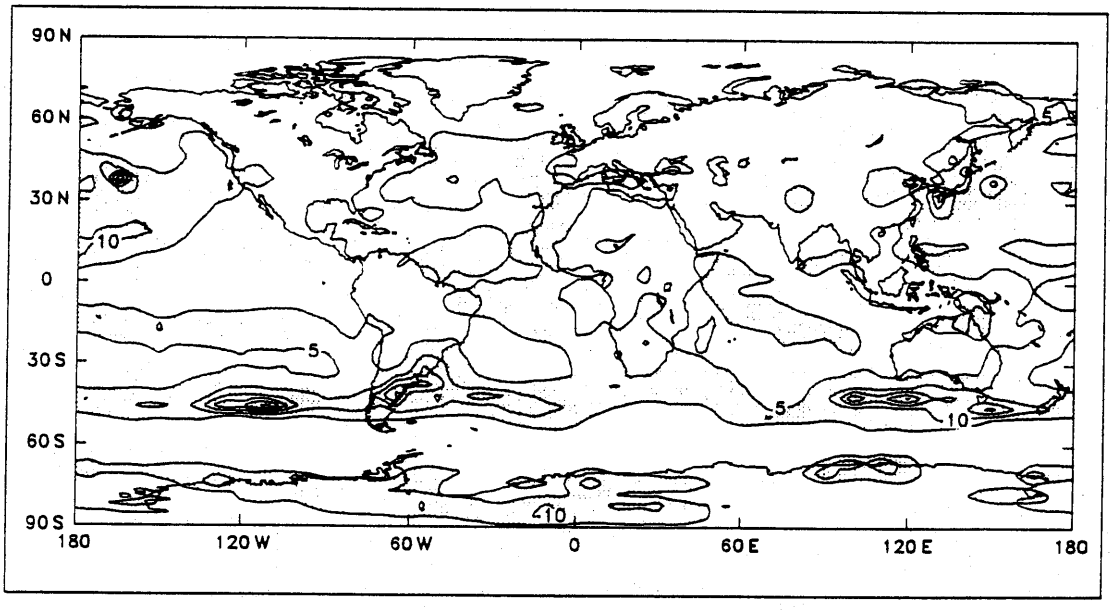

Figure 7: Model average of the $2xCO_2$ minus $1xCO_2$ change in precipitation rate ($\Delta\overline{P}$). Results are for DJF (a) and JJA (b), and are computed using equilibrium response data from five GCMs. The contour interval is 0.5 mm/day. Shading denotes areas where $\Delta\overline{P}$ is less than or equal to zero. The largest changes in $\Delta\overline{P}$ occur between 30°S to 30°N.

a

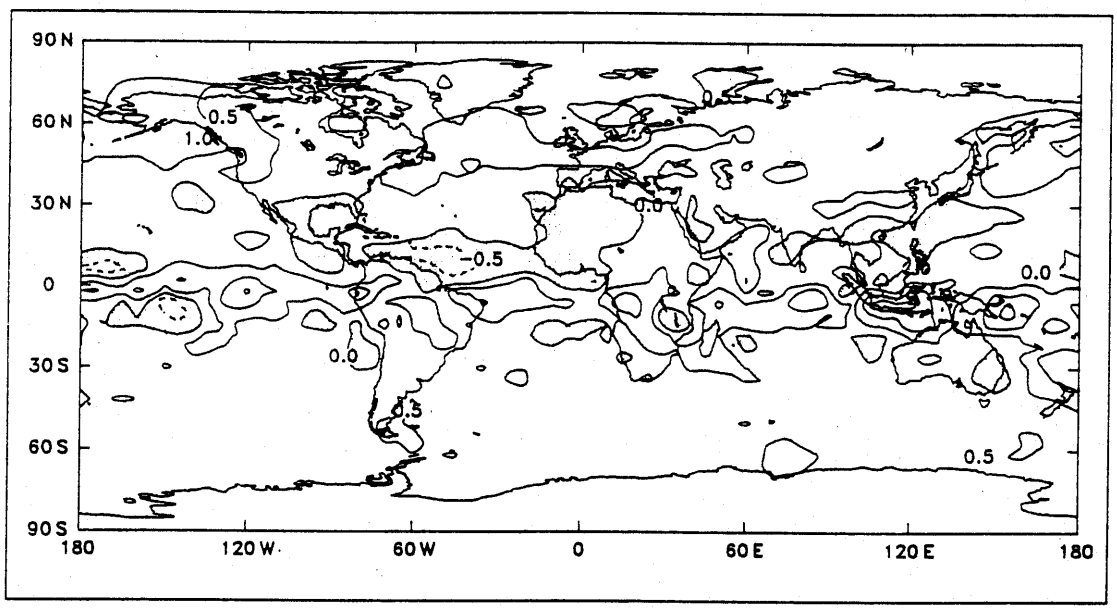

b

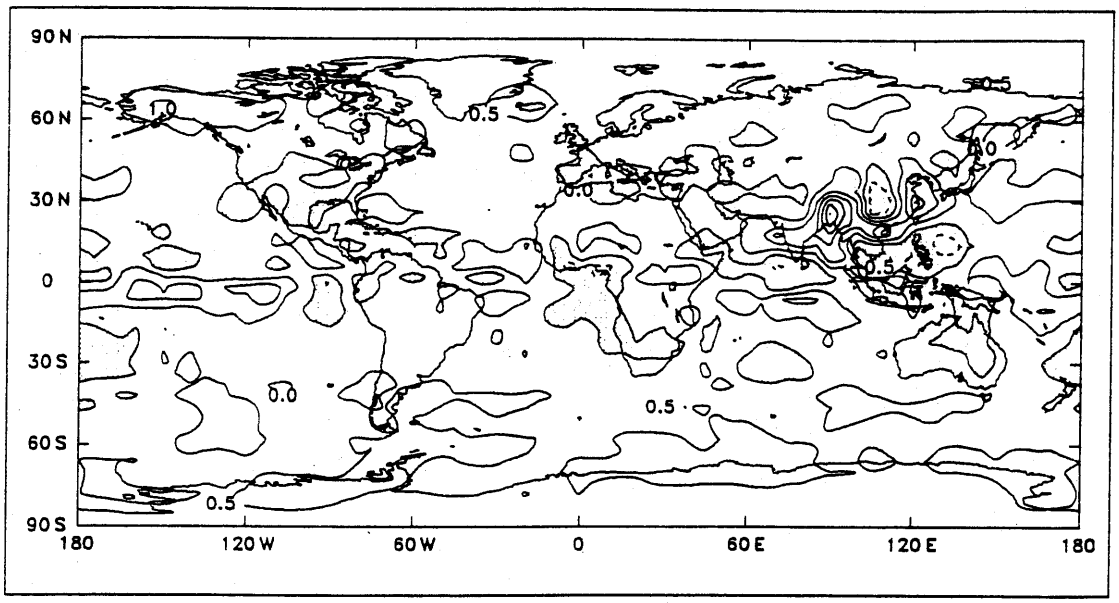

Figure 8: Model-to-model standard deviation ($\hat{s}_1$) of the $2xCO_2$ minus $1xCO_2$ change in precipitation rate (ΔP_i). Results are for DJF (a) and JJA (b), and are computed using equilibrium response data from five GCMs. The contour interval is 0.5 mm/day. Shading denotes areas where $\hat{s}_1$ is greater than or equal to 1.0.

a

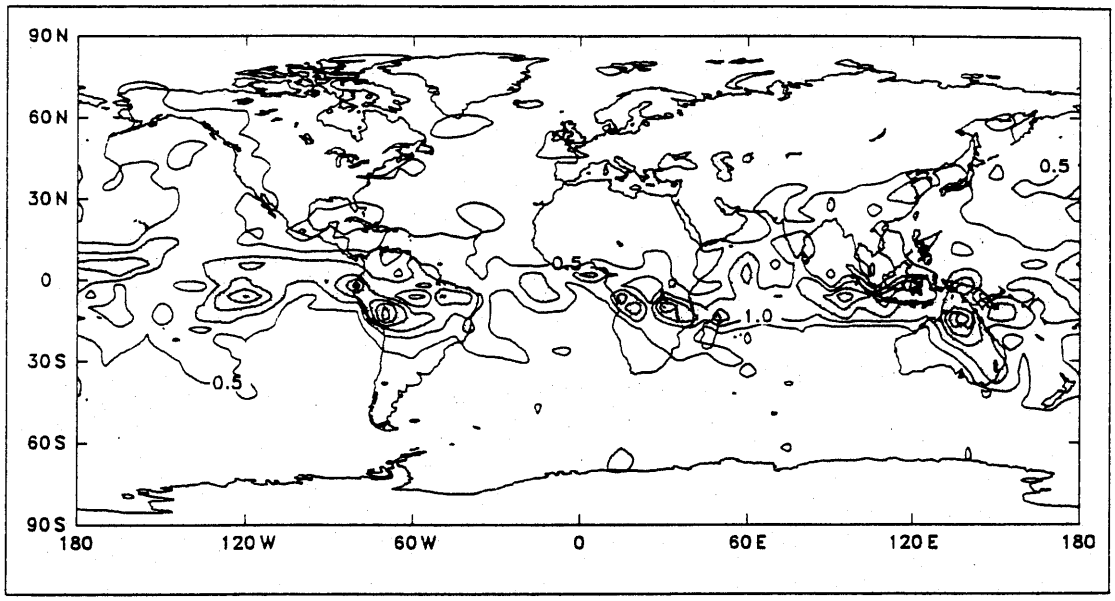

b

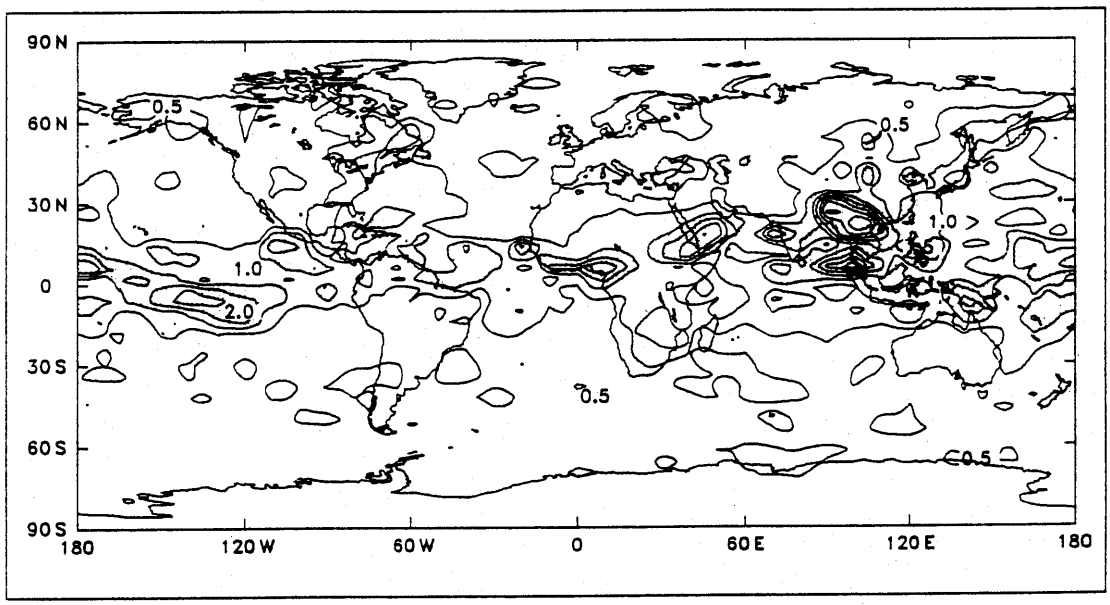

Figure 9: Probability of a decrease in precipitation rate ($p_{\Downarrow}$). For explanation, see Section 2.3. Results are for DJF (a) and JJA (b), and are computed using equilibrium response data from five GCMs. The contour interval is 0.25. Shading denotes areas where $p_{\Downarrow}$ is greater than or equal to 0.5, i.e., where the probability of a precipitation decrease is greater than or equal to one in two.

a

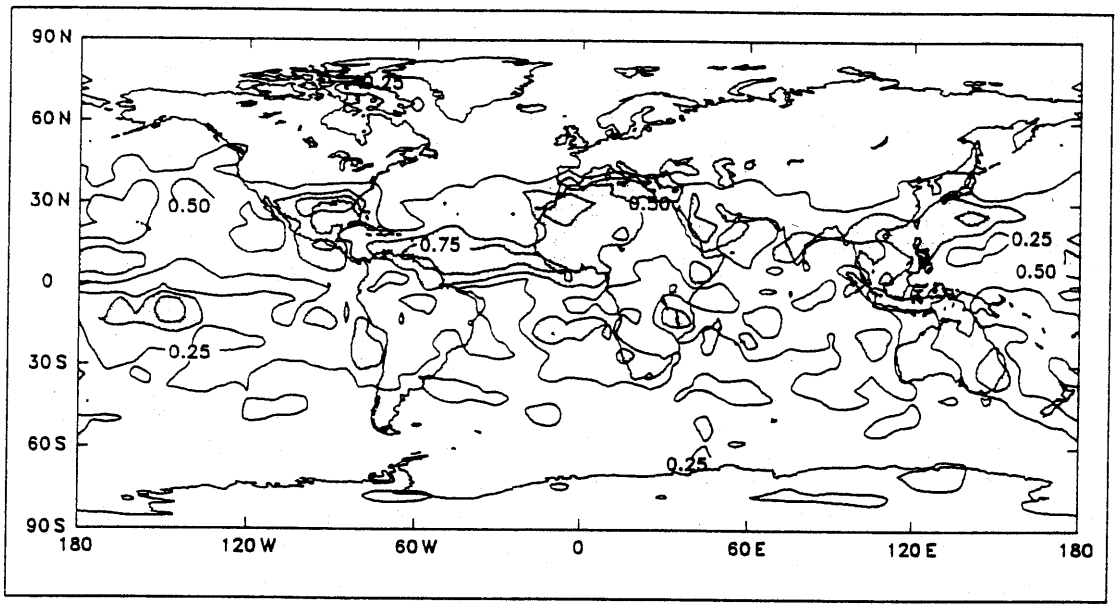

b

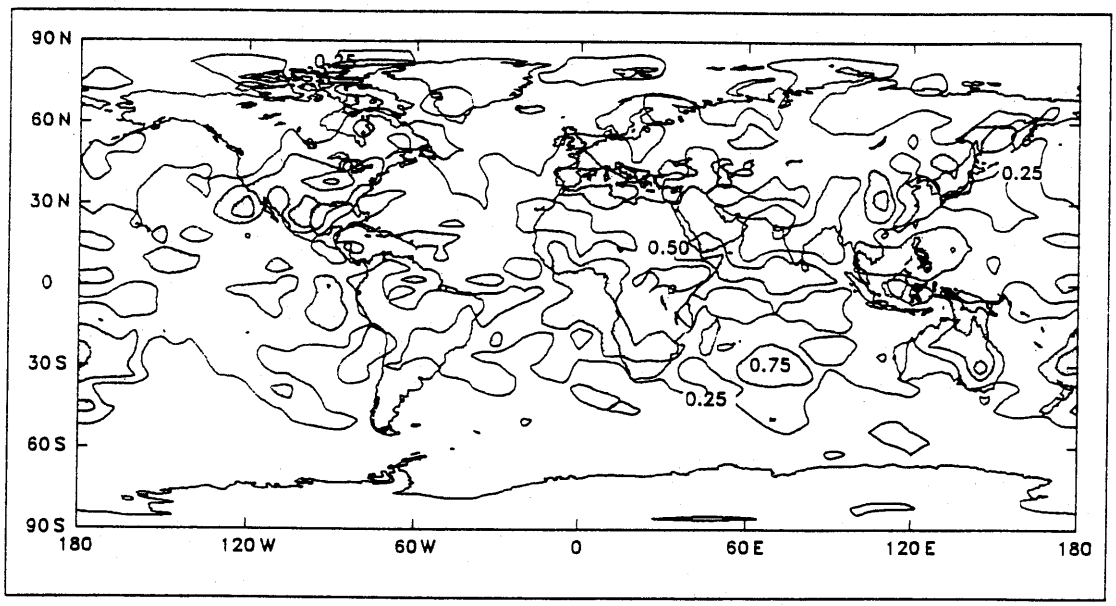

Figure 10: Model projections of global warming (from Wigley, 1989b). Results account for present levels of uncertainty for the climate sensitivity, ocean lag effects and the greenhouse gas forcing.

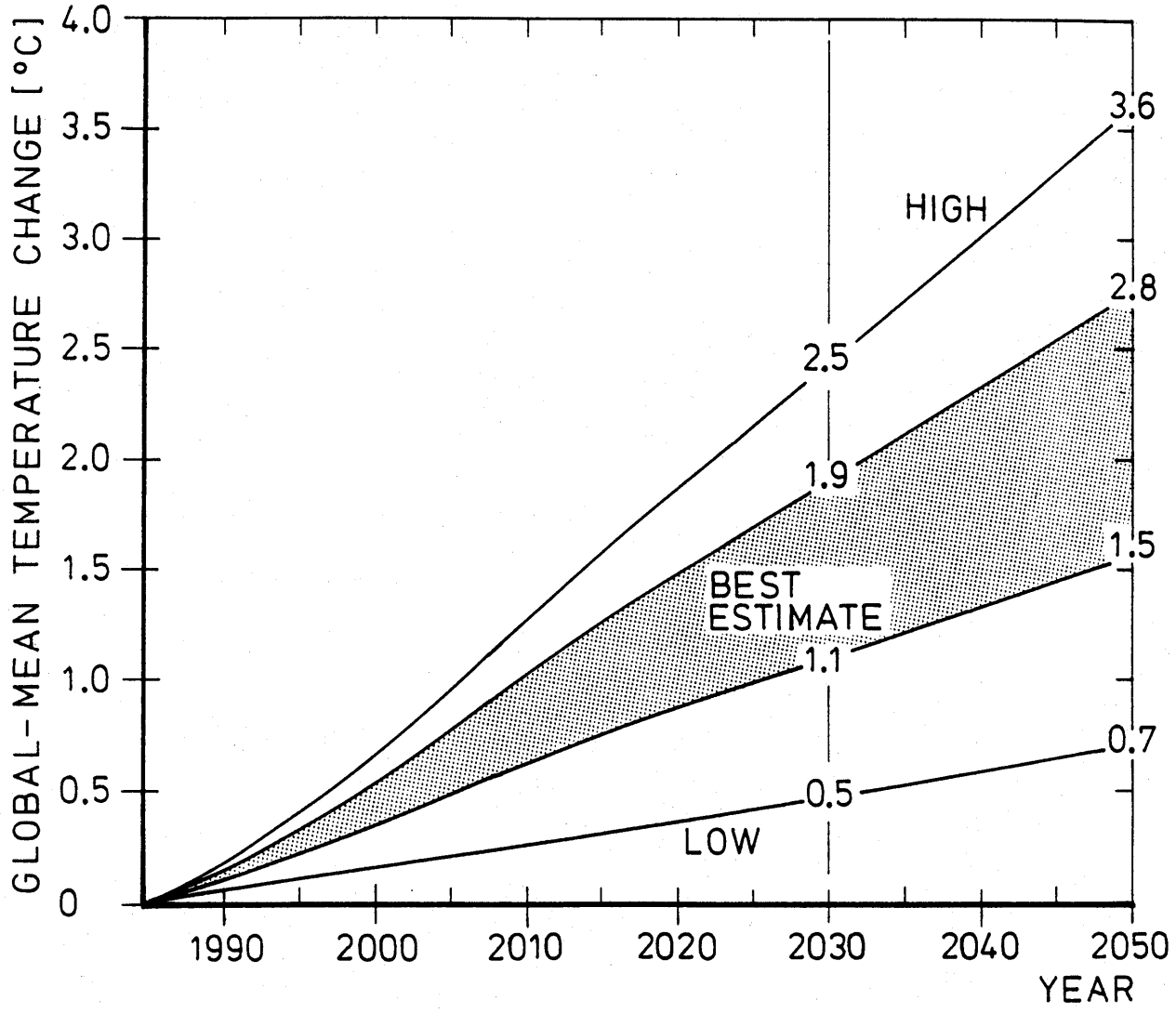

Figure 11: Model average of the $2xCO_2$ minus $1xCO_2$ change in surface air temperature ($\Delta\overline{T}$). Results are for DJF (a) and JJA (b) for a North American study area. The contour interval is 1°C. Shading denotes areas where $\Delta\overline{T}$ is greater than or equal to 4°C.

a

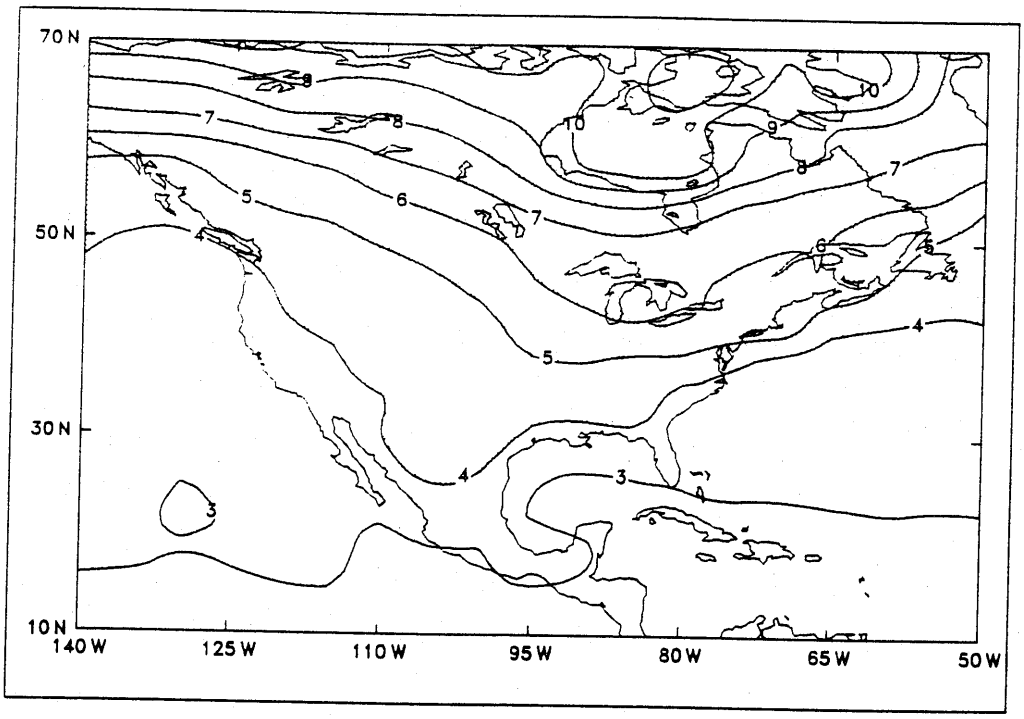

b

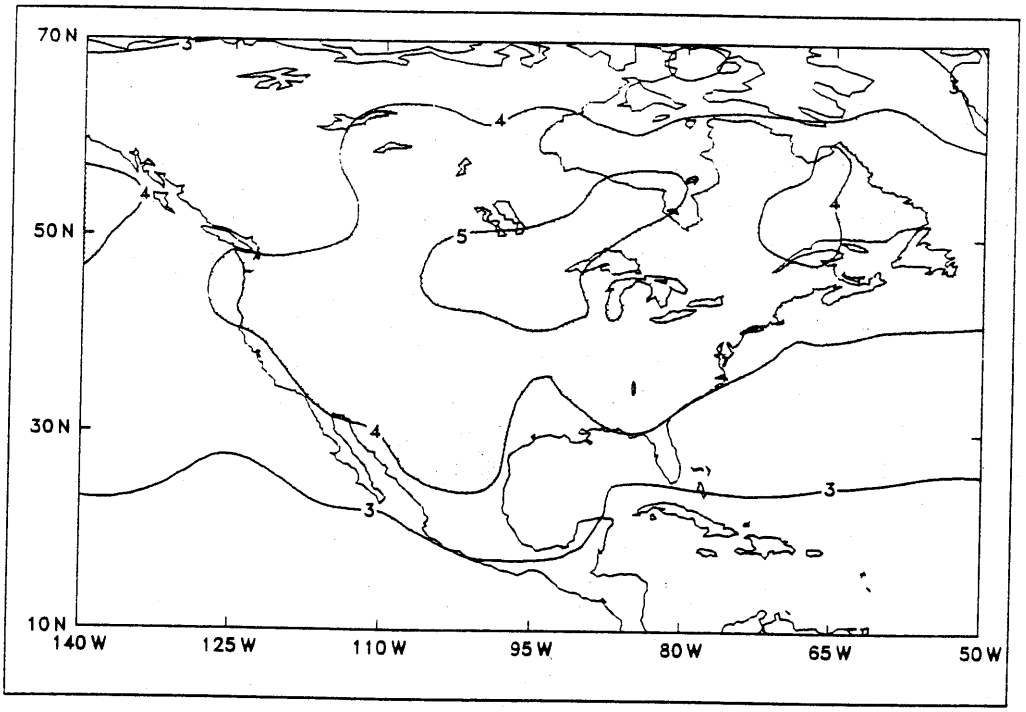

Figure 12: Standardized model average temperature change ($\Delta\overline{T}^*$) for DJF (a) and JJA (b). As for Figure 4 but for a North American study area. The contour interval is 0.25. Shading denotes areas where $\Delta\overline{T}^*$ is greater than or equal to 1.0.

a

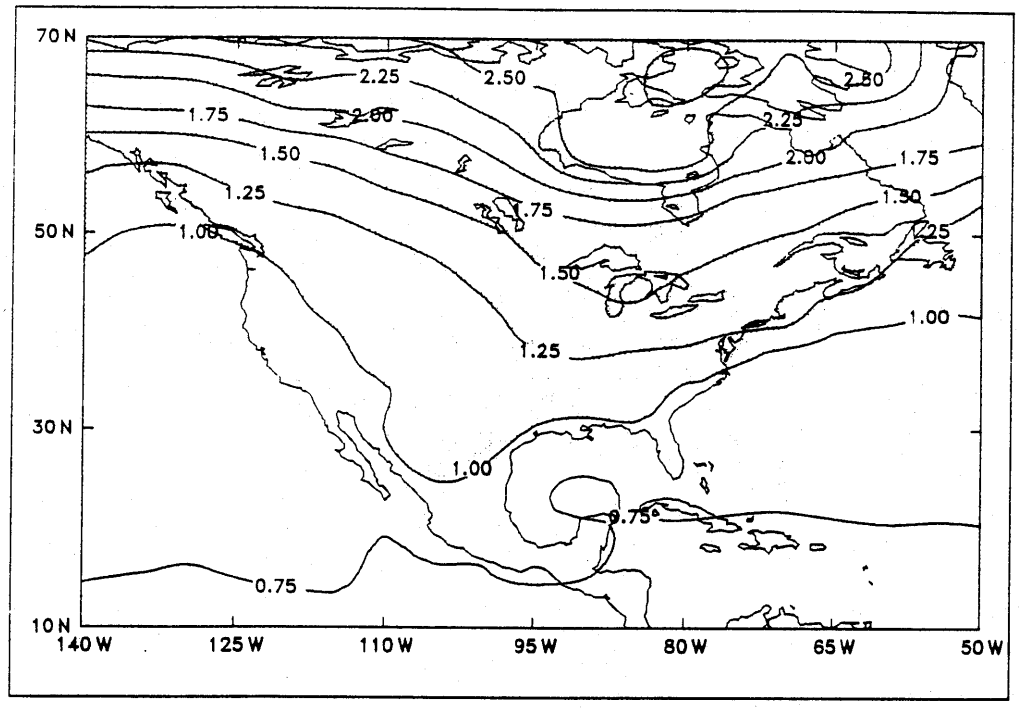

b

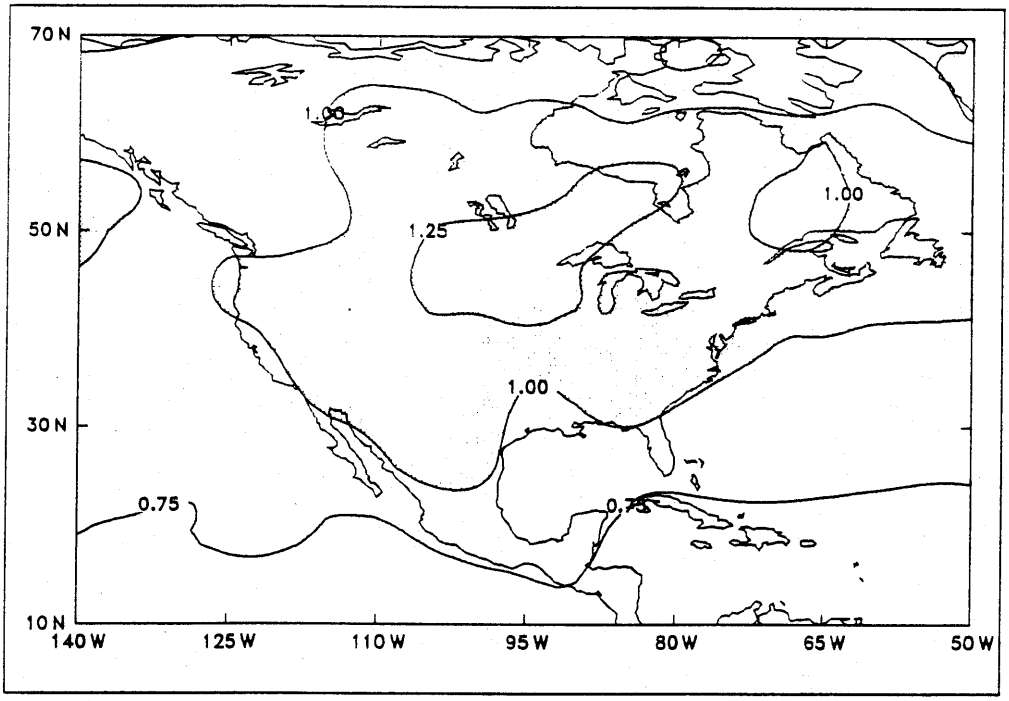

Figure 13: Signal-to-noise ratio SN2 for DJF (a) and JJA (b). As for Figure 6 but for a North American study area. The contour interval is 1.0. Shading denotes areas where SN2 is greater than or equal to 5.0.

a

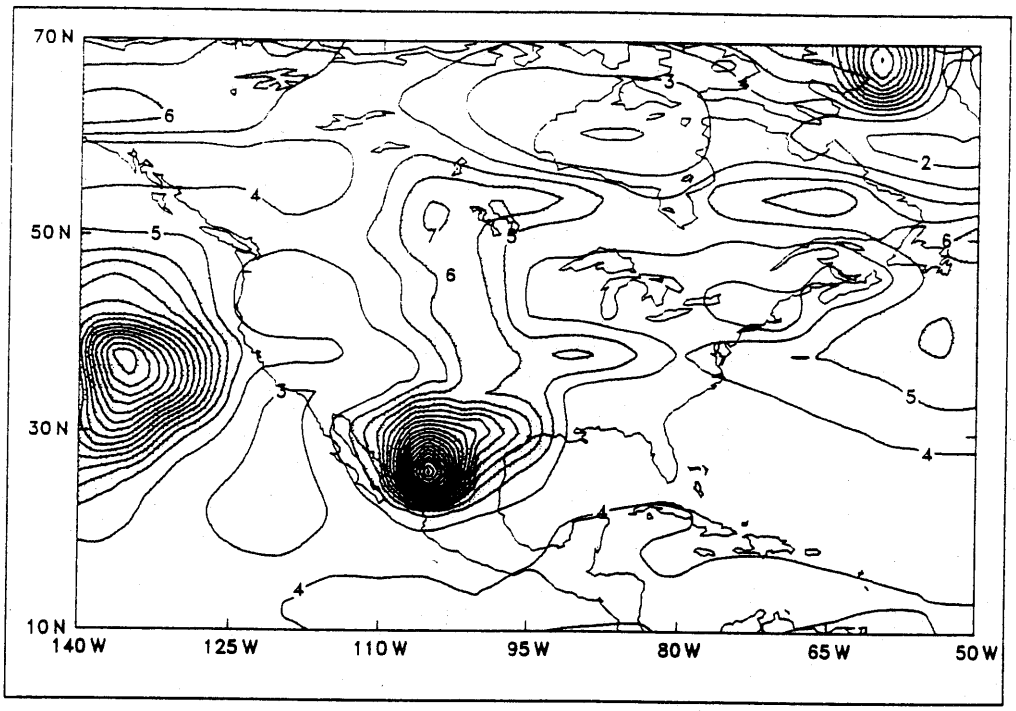

b

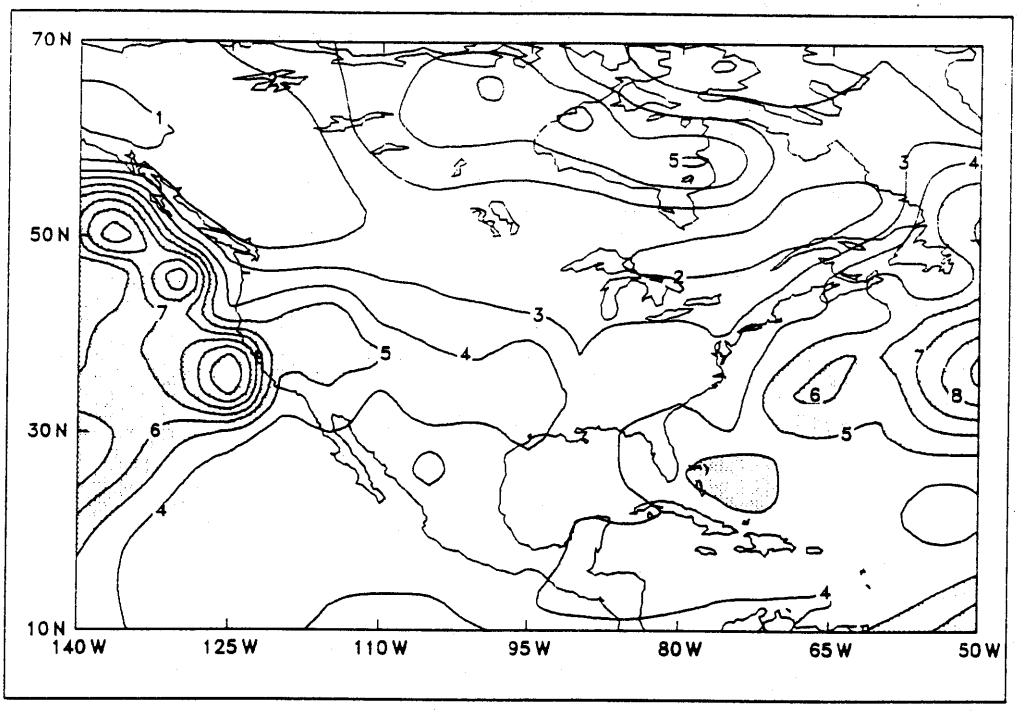

Figure 14: Probability of a decrease in precipitation rate ($p_{\downarrow}$) for DJF (a) and JJA (b). As for Figure 9 but for a North American study area. The contour interval is 0.1. Shading denotes areas where $p_{\downarrow}$ is greater than or equal to 0.5, i.e., where the probability of a precipitation decrease is greater than or equal to one in two.

a

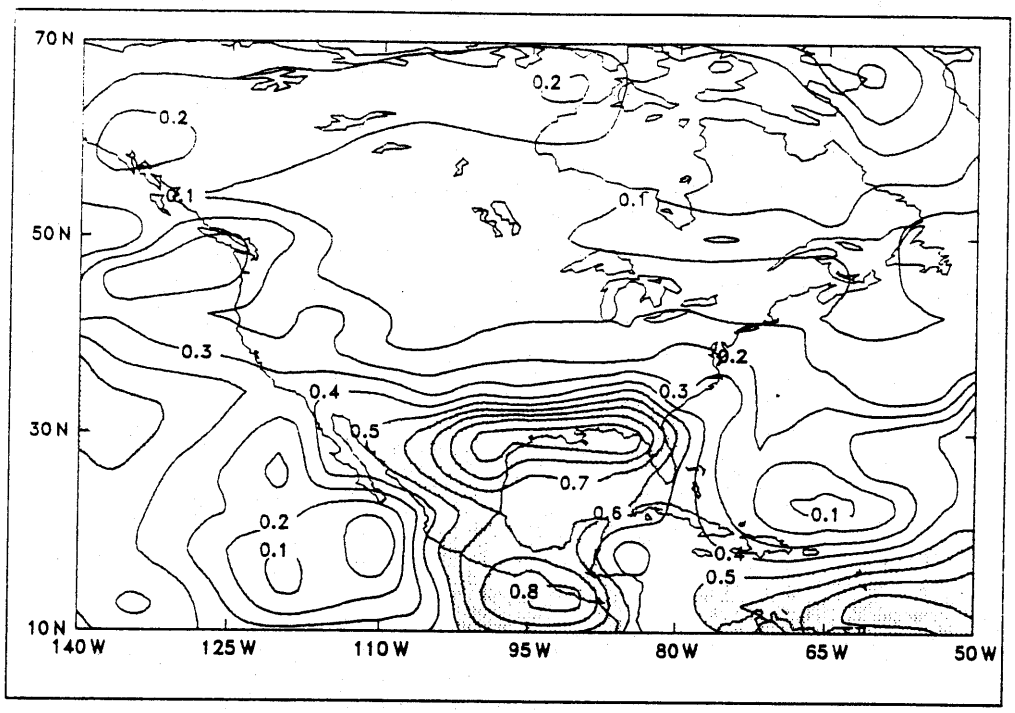

b

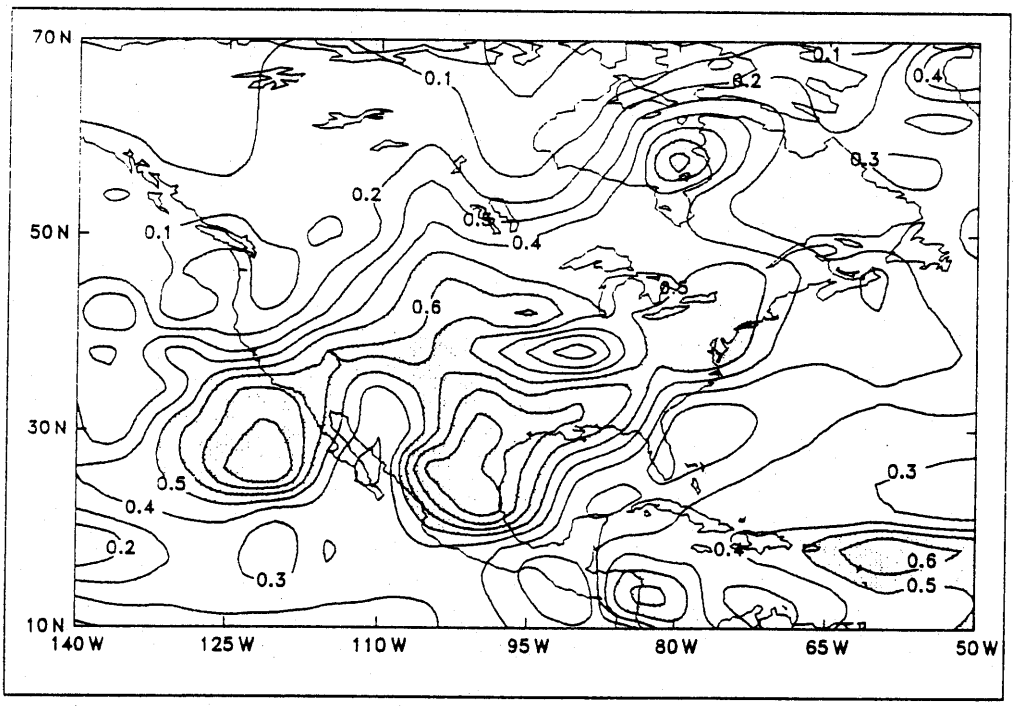

Figure 15: Model average of the $2xCO_2$ minus $1xCO_2$ change in surface air temperature ($\Delta\overline{T}$). Results are for DJF (a) and JJA (b) for a European study area. The contour interval is 1°C. Shading denotes areas where $\Delta\overline{T}$ is greater than or equal to 4°C.

a

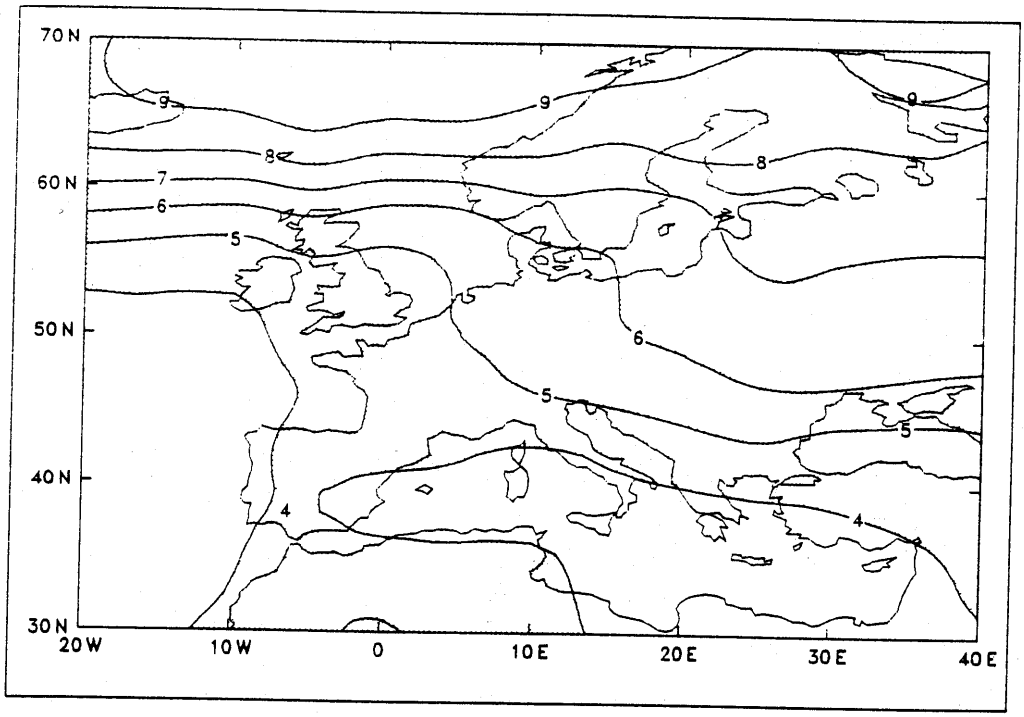

b

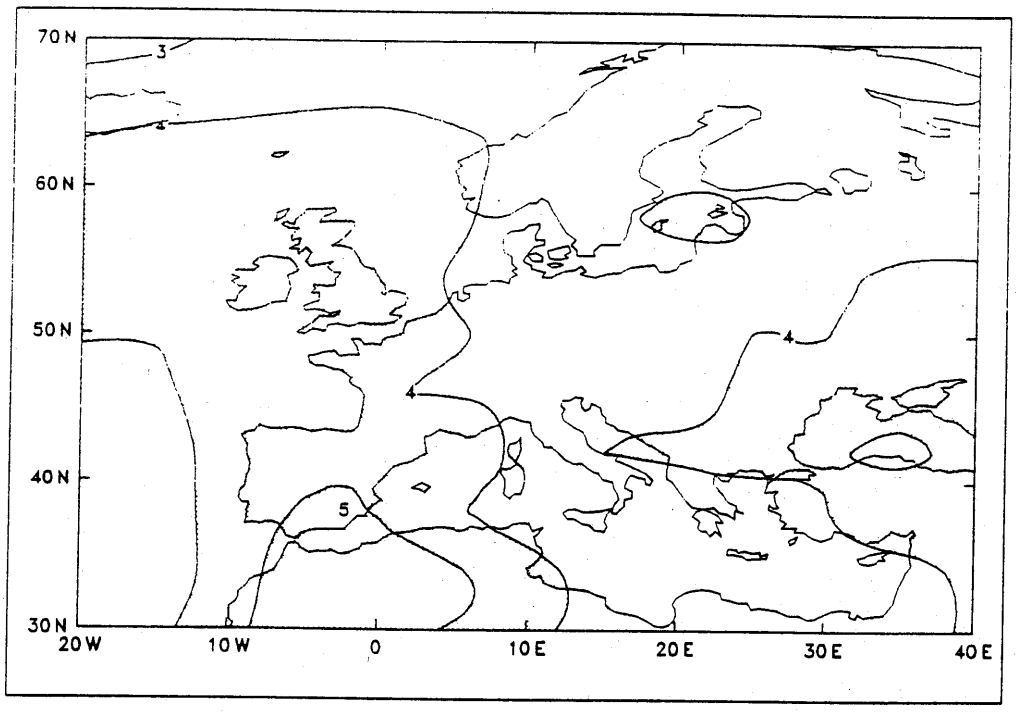

Figure 16: Standardized model average temperature change ($\Delta\overline{T}^*$) for DJF (a) and JJA (b). As for Figure 4 but for a European study area. The contour interval is 0.25. Shading denotes areas where $\Delta\overline{T}^*$ is greater than or equal to 1.0.

a

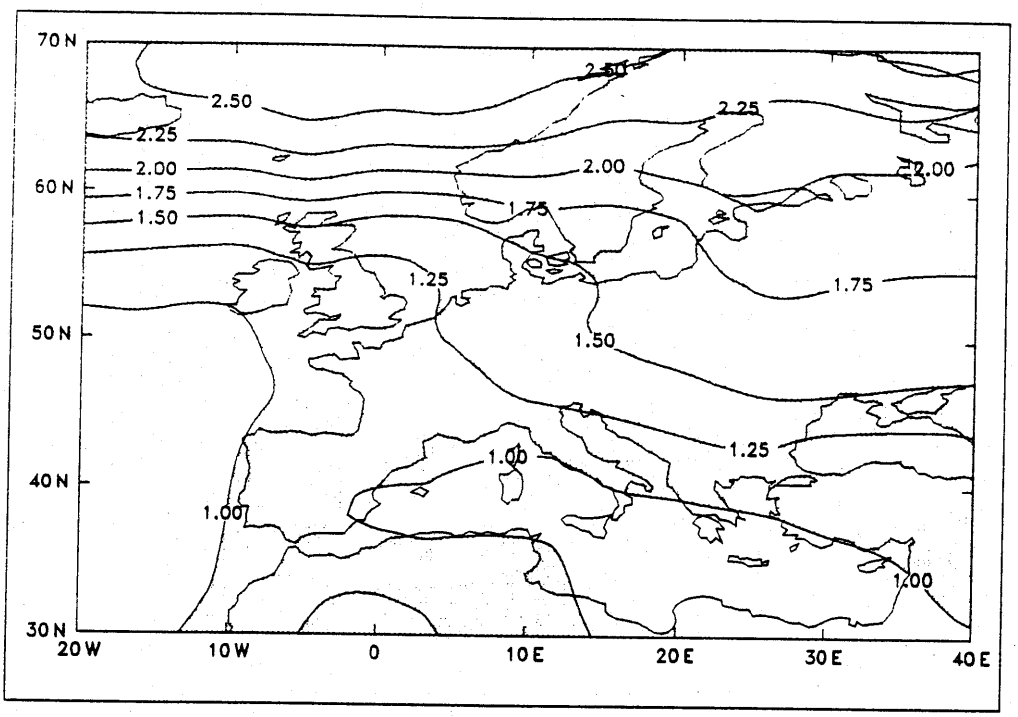

b

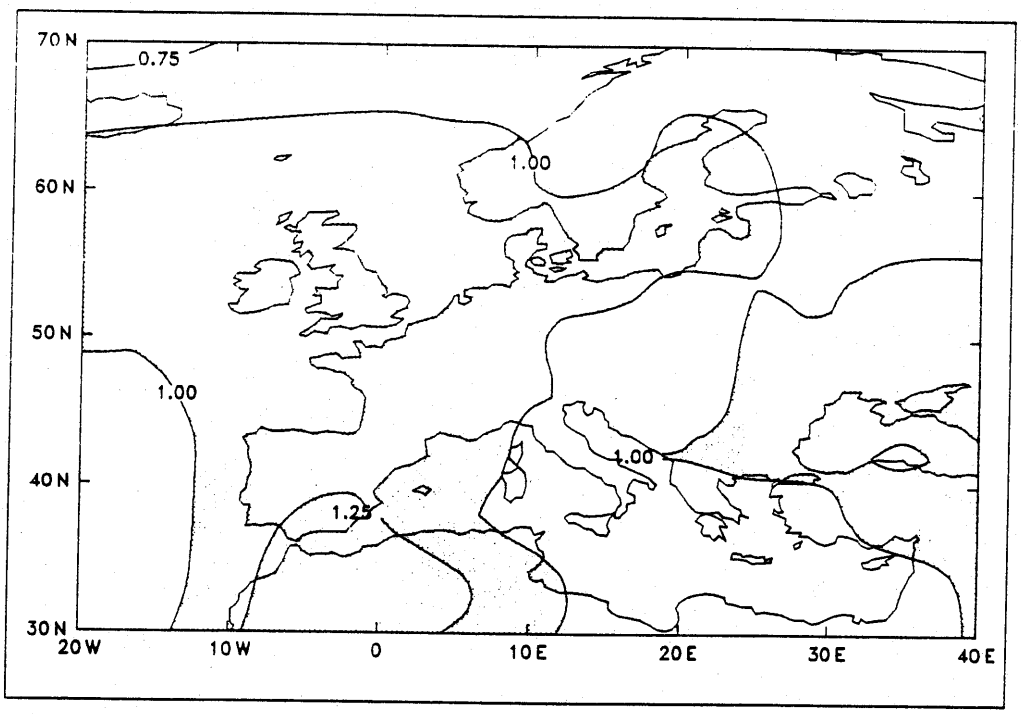

Figure 17: Signal-to-noise ratio SN2 for DJF (a) and JJA (b). As for Figure 6 but for a European study area. The contour interval is 1.0. Shading denotes areas where SN2 is greater than or equal to 5.0.

a

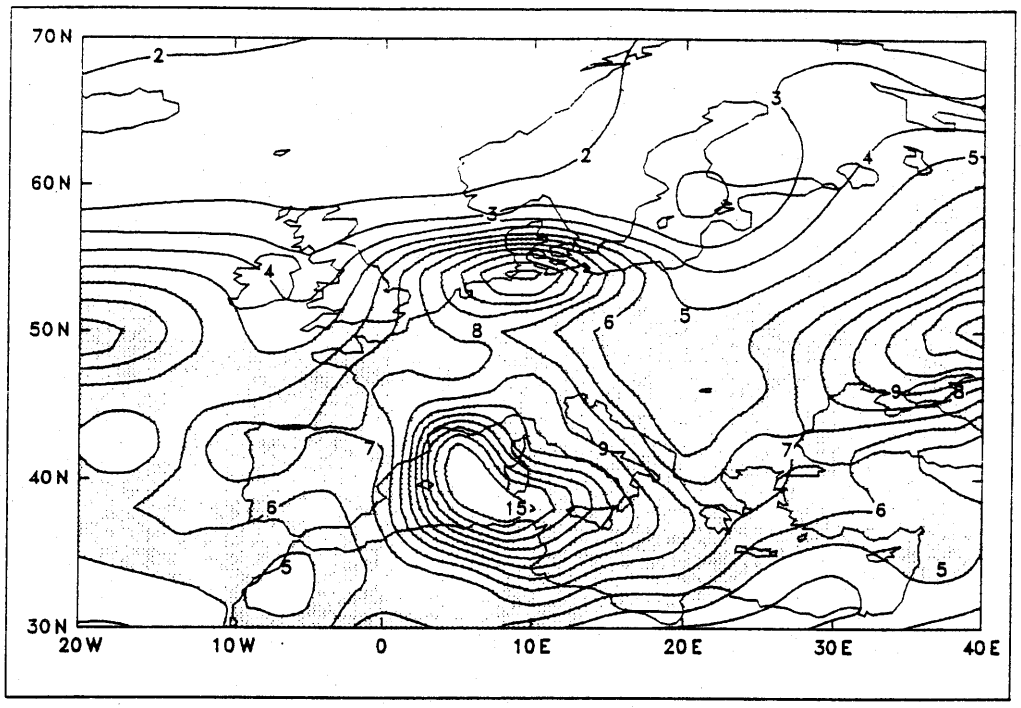

b

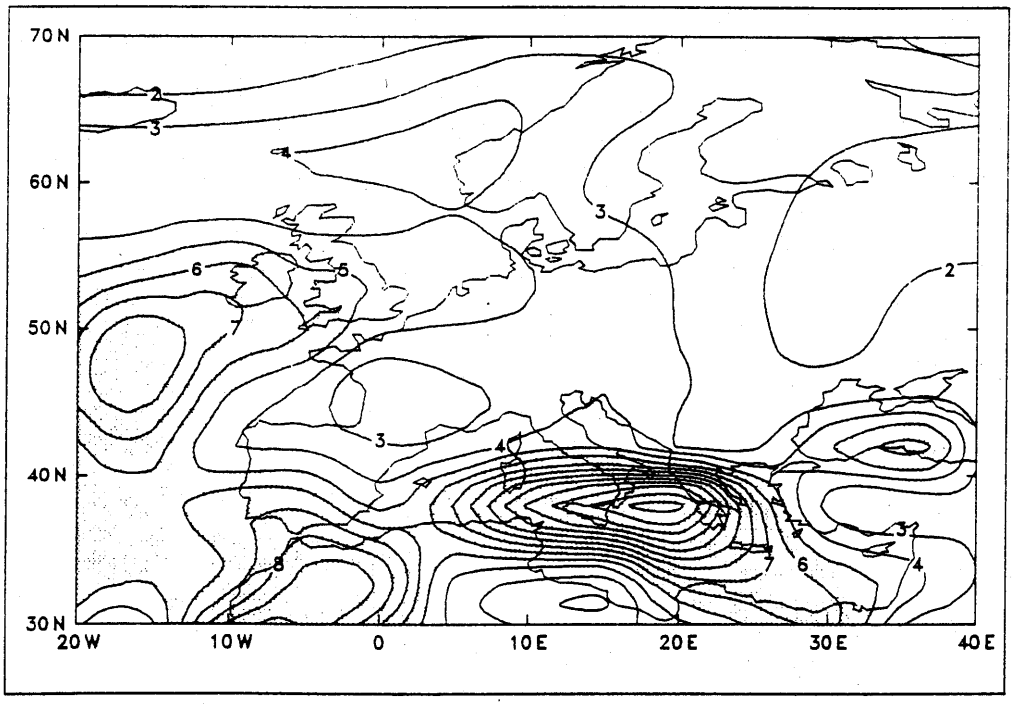

Figure 18: Probability of a decrease in precipitation rate ($p_{\downarrow}$) for DJF (a) and JJA (b). As for Figure 9 but for a European study area. The contour interval is 0.1. Shading denotes areas where $p_{\downarrow}$ is greater than or equal to 0.5, i.e., where the probability of a precipitation decrease is greater than or equal to one in two.

a

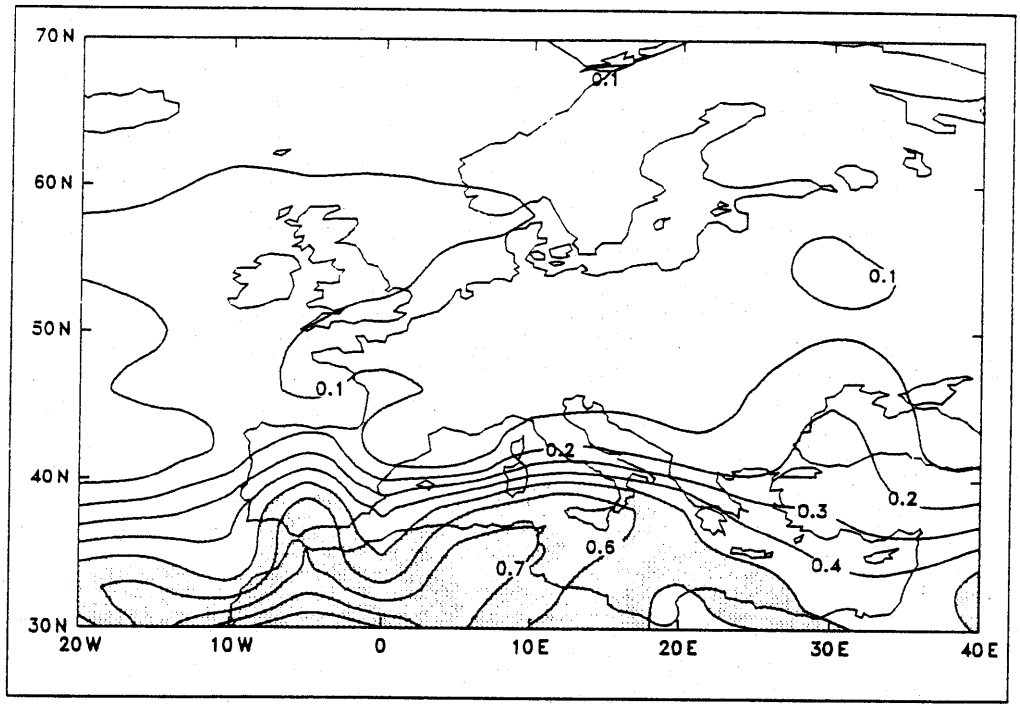

b